Monthly Notices
of the
ROYAL ASTRONOMICAL SOCIETY

MNRAS **466,** 2570–2589 (2017)
Advance Access publication 2016 December 10

doi:10.1093/mnras/stw3211

SDSS-IV MaNGA – the spatially resolved transition from star formation to quiescence

Francesco Belfiore,[1,2]★ Roberto Maiolino,[1,2] Claudia Maraston,[3] Eric Emsellem,[4,5] Matthew A. Bershady,[6] Karen L. Masters,[3,7] Dmitry Bizyaev,[8,9] Médéric Boquien,[10] Joel R. Brownstein,[11] Kevin Bundy,[12] Aleksandar M. Diamond-Stanic,[6,13] Niv Drory,[14] Timothy M. Heckman,[15] David R. Law,[16] Olena Malanushenko,[9] Audrey Oravetz,[9] Kaike Pan,[9] Alexandre Roman-Lopes,[17] Daniel Thomas,[3] Anne-Marie Weijmans,[18] Kyle B. Westfall[3] and Renbin Yan[19]

Affiliations are listed at the end of the paper

Accepted 2016 December 6. Received 2016 December 6; in original form 2016 June 1

ABSTRACT

Using spatially resolved spectroscopy from SDSS-IV MaNGA we have demonstrated that low ionization emission-line regions (LIERs) in local galaxies result from photoionization by hot evolved stars, not active galactic nuclei, hence tracing galactic region hosting old stellar population where, despite the presence of ionized gas, star formation is no longer occurring. LIERs are ubiquitous in both quiescent galaxies and in the central regions of galaxies where star formation takes place at larger radii. We refer to these two classes of galaxies as extended LIER (eLIER) and central LIER (cLIER) galaxies, respectively. cLIERs are late-type galaxies primarily spread across the green valley, in the transition region between the star formation main sequence and quiescent galaxies. These galaxies display regular disc rotation in both stars and gas, although featuring a higher central stellar velocity dispersion than star-forming galaxies of the same mass. cLIERs are consistent with being slowly quenched inside-out; the transformation is associated with massive bulges, pointing towards the importance of bulge growth via secular evolution. eLIERs are morphologically early types and are indistinguishable from passive galaxies devoid of line emission in terms of their stellar populations, morphology and central stellar velocity dispersion. Ionized gas in eLIERs shows both disturbed and disc-like kinematics. When a large-scale flow/rotation is observed in the gas, it is often misaligned relative to the stellar component. These features indicate that eLIERs are passive galaxies harbouring a residual cold gas component, acquired mostly via external accretion. Importantly, quiescent galaxies devoid of line emission reside in denser environments and have significantly higher satellite fraction than eLIERs. Environmental effects thus represent the likely cause for the existence of line-less galaxies on the red sequence.

Key words: galaxies: evolution – galaxies: fundamental parameters – galaxies: ISM.

1 INTRODUCTION

Large spectroscopic galaxy surveys (SDSS, York et al. 2000; zCOSMOS, Lilly et al. 2007; GAMA, Driver et al. 2011) have demonstrated that galaxies are strongly bimodal in several of their fundamental properties, including colours, star formation rates, stellar ages, morphology and gas content (Strateva et al. 2001; Blanton et al. 2003; Baldry et al. 2004, 2006; Schawinski et al. 2007; Wyder et al. 2007; Blanton & Moustakas 2009; Peng et al. 2010; Thomas et al. 2010). These observations support a scenario where some physical processes lead galaxies to transition from the 'star-forming' (SF) blue cloud to the passive 'red sequence', causing the eventual shutdown (or 'quenching') of star formation on a galaxy-wide scale.

The physics driving this transformation is currently hotly debated and has not yet been unambiguously identified, although it is likely that more than one mechanism is at play (Schawinski et al. 2007;

★ E-mail: fb338@cam.ac.uk

© 2016 The Authors
Published by Oxford University Press on behalf of the Royal Astronomical Society

Downloaded from https://academic.oup.com/mnras/article/466/3/2570/2666397 by INAF Trieste (Osservatorio Astronomico di Trieste) user on 25 November 2020

Peng et al. 2010; Mendel et al. 2013; Schawinski et al. 2014; Peng, Maiolino & Cochrane 2015; Smethurst et al. 2015). A growing body of evidence points towards at least two quenching pathways: an *environment-dependent* channel, acting differentially on central and satellite galaxies and a *mass-dependent* channel, which may be associated with internal processes (Rees & Ostriker 1977; Silk 1977; Kauffmann et al. 2006). This inference is supported by the separability of the effects of mass and environment on the passive fraction (Baldry et al. 2006; Peng et al. 2010; Thomas et al. 2010). These two quenching pathways have each been associated with several physical processes: ram pressure stripping (Larson, Tinsley & Caldwell 1980), harassment and strangulation (Gunn & Gott 1972; Peng et al. 2015) for the environment-related channel and radio mode feedback from active galactic nuclei (AGN, Croton et al. 2006; Dekel & Birnboim 2006; Cattaneo et al. 2009), halo mass shock heating (Birnboim & Dekel 2003; Keres et al. 2005; Dekel & Birnboim 2006; Keres et al. 2009) or morphological quenching (Martig et al. 2009; Forbes et al. 2014; Genzel et al. 2014) for the mass-dependant channel. It has also been suggested that both mass and environmental quenching may be manifestations of the same quenching channel (Carollo et al. 2014; Knobel et al. 2015).

Observationally much work has been dedicated to the study of environmental effects, demonstrating that local environment correlates well with morphology (e.g. Dressler 1980; Bamford et al. 2009), colour (Blanton et al. 2005b; Baldry et al. 2006; Peng et al. 2010) or gas content (Cortese et al. 2011; Boselli, Cortese & Boquien 2014). The direct effect of the hot cluster atmosphere on infalling galaxies (ram pressure stripping) is further observed both via trails of H I (e.g. Chung et al. 2009) and ionized gas (e.g. Fumagalli et al. 2014; Poggianti et al. 2016).

Regarding the mass quenching regime, the observational picture is much more complex. Several studies agree on the fact that the presence of a massive bulge is the single best observational parameter correlating with the probability of a galaxy to be passive (Cheung et al. 2012; Pasquali, Gallazzi & van den Bosch 2012; Wake, van Dokkum & Franx 2012; Bluck et al. 2014). Since black hole mass is correlated to the bulge mass (Marconi & Hunt 2003; Häring & Rix 2004; McConnell & Ma 2013), it can be expected that galaxies with more massive bulges experience a larger amount of energetic feedback from their black holes. The details of the coupling between the black hole and its host galaxy are, however, not currently understood. As recently reviewed by Heckman & Best (2014), AGN appear as a bimodal population that can be broadly divided into radiative-mode (including Seyfert galaxies and quasars) and radio-mode AGN. In the low-redshift Universe, no direct correlation is observed between radiative-mode AGN and the shutdown of star formation, as radiative-mode AGN are often associated with the presence of star formation in the central regions of galaxies (inner few kpc). While radiative-mode AGN are observed to power large-scale outflows (Maiolino et al. 2012; Cicone et al. 2014; Carniani et al. 2015), the duty cycle and time-scales of these phenomena is uncertain, thus making their impact on the exhaustion of the cold gas reservoir in galaxies questionable. Radio mode AGN, on the other hand, are observed to inflate large bubbles of ionized gas in massive haloes, thus playing an important contribution to offsetting the cooling of the gas in the halo (Fabian 2012). The extension of this feedback mechanisms to lower masses (halo mass $<10^{12}\,M_{\odot}$) is observationally uncertain.

Both environmental and mass quenching (through radio-mode AGN heating) channels are included in recent semi-analytical models (Bower et al. 2006; Croton et al. 2006) and in cosmological hydrodynamical simulations via sub-grid prescriptions (Gabor & Davé 2012; Schaye et al. 2014; Vogelsberger et al. 2014) in order to match the stellar mass function and the bimodality of the observed galaxy population. In recent years, models of galaxy formation and evolution have become able to qualitatively reproduce the main features of the bimodal galaxy population (e.g. Sales et al. 2014; Trayford et al. 2016). Namely, in simulations environmental quenching appears to be the main cause of growth of the red sequence at low masses, while AGN radio-mode heating is responsible for the presence of high-mass central passive galaxies. However, while qualitative agreement with observations is promising, this success does not imply that the sub-grid recipes implemented for AGN feedback are physically correct.

Observationally, further insight into the quenching process could be obtained by a statistical study of how it proceeds inside galaxies: 'inside out' versus 'outside in' scenarios (e.g. Li et al. 2015; Tacchella et al. 2015), and what role the different morphological components (disc, bar, bulge) have in the process (Martig et al. 2009; Masters et al. 2012). Current integral field spectroscopy (IFS) galaxy surveys (CALIFA, Sánchez et al. 2012; SAMI, Allen et al. 2015; MaNGA, Bundy et al. 2015) promise to revolutionize the observational picture, by enabling the study of the relation between star formation and quiescence on resolved scales. Nebular emission lines, originating from SF regions, are the ideal tool to trace current ($<$100 Myr old) star formation on the kpc scales (Kennicutt 1998) probed by a survey like MaNGA (mean redshift $\langle z\rangle \sim 0.03$), provided other contributions to line emission (AGN, old hot stars etc.) can be disentangled.

In this paper, we make use of a large sample of $\sim$600 galaxies observed as part of the Sloan Digital Sky Survey IV (Blanton et al., submitted) Mapping Nearby Galaxies at Apache Point Observatory (SDSS-IV MaNGA) survey, and build on the analysis presented in Belfiore et al. (2016) to define spatially resolved 'quiescence' and make an unbiased census of SF and quiescent regions within the $z\sim 0$ galaxy population. This work is structured as follows. In Section 2, we briefly recap the relevant properties of the MaNGA data and our spectral fits. In Section 3, we summarize the main findings of Belfiore el al. (2016, hereafter Paper I), including our new emission-line-based galaxy classification, the importance of low ionization emission-line regions (LIERs) in the context of understanding quiescence in galaxies and the stellar populations properties of the different galaxy classes. In Section 4, we explore the role of LIER galaxies within the bimodal galaxy population, while in Section 5 we gather evidence regarding the origin of the ionized gas in LIERs. Finally in Section 6, we discuss possible evolutionary scenarios for LIER galaxies. We conclude in Section 8.

Throughout this work redshifts, optical and UV photometry and stellar masses are taken from the MaNGA targeting catalogue, based on an extended version of the NASA Sloan Atlas (NASA-Sloan catalogue) (NSA `v1_0_1`,[1] Blanton et al. 2011). Stellar masses are derived using a Chabrier (2003) initial mass function and using the `kcorrect` software package (version `v4_2`, Blanton & Roweis 2007) with Bruzual & Charlot (2003) simple stellar population models. All quoted magnitudes are in the AB system and *k*-corrected to rest frame after correction for galactic extinction. Effective radii are measured from the SDSS photometry by performing a Sérsic fit in the *r* band. Single fibre spectroscopic data from the SDSS Legacy Survey data release 7 (Abazajian et al. 2009) for the main galaxy sample targets (Strauss et al. 2002) are referred to as legacy SDSS. When quoting luminosities, masses and

[1] http://www.sdss.org/dr13/manga/manga-target-selection/nsa/

Downloaded from https://academic.oup.com/mnras/article/466/3/2570/2666397 by INAF Trieste (Osservatorio Astronomico di Trieste) user on 25 November 2020

distances we make use of a ΛCDM cosmology with $\Omega_m = 0.3$, $\Omega_\Lambda = 0.7$ and $H_0 = 70\,\mathrm{km^{-1}\,s^{-1}\,Mpc^{-1}}$.

2 THE MANGA DATA

MaNGA (Bundy et al. 2015; Yan et al. 2016a) is an IFS survey, making use of the SDSS 2.5 m telescope at Apache Point Observatory (Gunn et al. 2006), aimed at obtaining spatially resolved spectroscopy for 10 000 nearby galaxies in the redshift range $0.01 < z < 0.15$. Observations are obtained using purpose-built hexagonal integral field units (IFUs, Drory et al. 2015), assembled from 2 arcsec diameter fibres, which are fed to the dual beam BOSS spectrographs covering the wavelength range 3600 to 10 300 Å with a spectral resolution $R \sim 2000$ (Smee et al. 2013). The size distribution of the IFUs is optimized to match the size and density of galaxy targets on the sky (Wake at al. in preparation), in order to cover 2/3 of the targets to 1.5 effective radii (R_e) and 1/3 of the targets to 2.5 R_e. The MaNGA sample is selected to be flat in *i*-band absolute magnitude. At each *i*-band magnitude (and thus approximately in each stellar mass bin), the MaNGA primary and secondary samples are selected to be volume limited within a prescribed redshift range.

Seventeen galaxy IFUs (ranging from 19-fibre IFU, 12 arcsec on sky diameter, to 127-fibre IFU, 32 arcsec on sky diameter) are observed simultaneously, together with a set of twelve 7-fibre mini-bundles used for flux calibration (Yan et al. 2016b) and 92 single fibres for sky subtraction. A three-point dithering pattern is used during observations to compensate for light loss and obtain a uniform point spread function (PSF, Law et al. 2015). The MaNGA data were reduced using version `v1_3_3` of the MaNGA reduction pipeline (Law et al. 2016). The wavelength calibrated, sky subtracted and flux calibrated MaNGA fibre spectra (error vectors and mask vectors) and their respective astrometric solutions are combined to produce final datacubes with pixel size set to 0.5 arcsec. The median PSF of the MaNGA datacubes is estimated to have a full width at half-maximum (FWHM) of 2.5 arcsec. The MaNGA sample has been demonstrated to be well suited for studies of gas physics and stellar population properties of nearby galaxies as shown in preliminary analysis of data from the MaNGA prototype instrument (Belfiore et al. 2015; Li et al. 2015; Wilkinson et al. 2015).

Physical parameters of the continuum and the emission lines are obtained via a customized spectral fitting procedure described in Paper I (Section 2.2). In short, spaxels are binned for optimizing the S/N ratio in the continuum, which is then fitted with a set of MIUSCAT simple stellar population templates (Vazdekis et al. 2012) via the penalized pixel fitting routine (Cappellari & Emsellem 2004). Subsequently a new binning is performed, optimizing the Hα S/N, which is used to fit nebular emission lines. Emission lines are fitted as sets of Gaussians (one per line) with a common velocity. Further constrains are imposed on lines originating from the same ion.

3 LIER EMISSION IN GALAXIES: CLASSIFICATION AND OPEN QUESTIONS

3.1 Paper I: a revised classification scheme based on spatially resolved diagnostic diagrams

In Paper I, we investigated the spatial distribution and properties of galactic regions that are classified as 'LINERs' (low ionization nuclear emission-line regions) in the conventional [S II] λλ6717, 6731/Hα versus [O III] λ5007/Hβ BPT (Baldwin, Phillips & Terlevich 1981) diagnostic diagram. We showed that such regions are not nuclear, but distributed on large (kpc) scales, hence motivating the relabelling of these regions as 'LIERs' (i.e. dropping the 'N', which stood for 'nuclear', from the historical acronym). We made use of different lines of evidence to argue against the AGN origin of LIER emission, instead supporting the scenario where LIERs are caused by photoionization from a diffuse ionizing background produced by hot evolved stars.

More specifically we summarize the main conclusions of Paper I as follows:

(i) LIER emission is spatially strongly correlated with absence of young stellar populations [as traced by stellar indices like $D_N(4000)$ and $H\delta_A$].

(ii) Post-asymptotic giant branch (pAGB) stars have been shown to produce the required hard ionizing spectrum necessary to excite LIER emission (Binette et al. 1994; Stasińska et al. 2008). Stellar evolution models including the pAGB phase demonstrate that the pAGB hypothesis is energetically viable for virtually all LIERs, as the observed EW(Hα) lie in the same range as model predictions (0.5–3.0 Å).

(iii) Although weak AGN may appear as true LINERs when observed on scales of 100 pc or less, a typical low luminosity AGN does not emit enough energy to be the dominant contributor to the ionizing flux on the kpc scales probed by the 3 arcsec SDSS fibre (from the legacy SDSS, $\langle z \rangle \sim 0.1$) or by MaNGA ($\langle z \rangle \sim 0.03$).

(iv) In LIER galaxies not contaminated by SF, line ratios sensitive to the ionization parameter ([O III] λ5007/[O II] λ3727 and partially [O III] λ5007/Hβ) show flat or very shallow profiles over radial scales of tens of kpc, at odds with the steeper profiles predicted in the AGN scenario.

(v) The distribution of EW(Hα) in LIERs is flat as a function of galactocentric radius and presents a remarkably small scatter, as expected in the case of nebular lines being excited by hot evolved stars associated with the old stellar population. On the other hand, in the AGN scenario, a large scatter is expected in the EW(Hα) distribution, as line and stellar continuum emission would originate from independent sources.

While previous work has associated LIER emission in red (elliptical) galaxies with pAGB stars (Binette et al. 1994; Sarzi et al. 2010; Yan & Blanton 2012; Singh et al. 2013), we note that *Hubble Space Telescope* imaging of very nearby elliptical galaxies struggles to account for the number of UV bright (especially pAGB) stars predicted by stellar population models (Brown et al. 1998, 2008; Rosenfield et al. 2012). If models have substantially overestimated the occurrence of pAGB stars, other hot evolved stars (most notably extreme horizontal branch stars) may represent a more sizeable contribution to the ionizing photon budget leading to LIER emission. For the purposes of this paper, the exact nature of the evolved stellar sources powering the LIER emission does not affect any of the conclusions.

In this framework LIERs are direct tracers of regions dominated by old stellar populations where, despite the presence of gas, star formation is no longer taking place. Importantly, LIERs appear both in red sequence galaxies, which host no current star formation, but also in the central regions of spiral galaxies, where star formation actively takes place at larger galactocentric radii (as recently highlighted by the contributions from the CALIFA survey, Singh et al. 2013; Gomes et al. 2016). We refer to these two classes of galaxies 'extended LIER' (eLIER) and 'central LIER' (cLIER), respectively, with the absence or presence of SF regions being the discriminating factor. Examples of galaxies in each class are given in Fig. 1, together with maps of their line emission (Hα flux and EW), age-sensitive stellar population indices [$D_N(4000)$ and $EW(H\delta_A)$]

Downloaded from https://academic.oup.com/mnras/article/466/3/2570/2666397 by INAF Trieste (Osservatorio Astronomico di Trieste) user on 25 November 2020

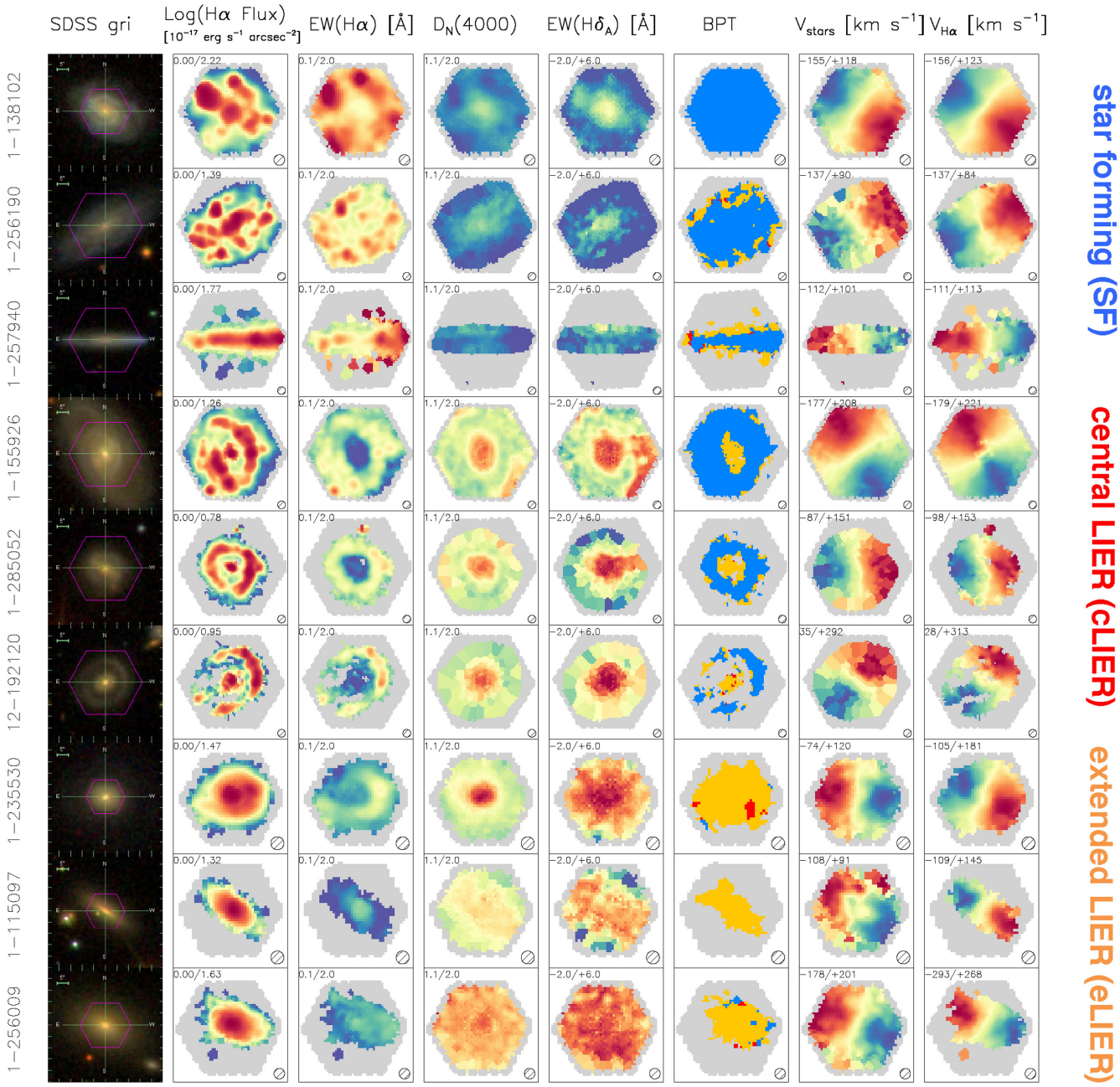


Figure 1. Example of the different properties of SF (top three), cLIER (middle three) and eLIER (bottom three) galaxies. Each row represents a different galaxy (labelled with its MaNGA-ID on the left). The columns represent, respectively (1) SDSS $g-r-i$ composite image with MaNGA bundle superimposed, (2) MaNGA Hα map, (3) MaNGA EW(Hα) map, (4) MaNGA map of $D_N(4000)$, (5) MaNGA map of Hδ_A, (6) BPT map of the MaNGA galaxies based on the [S II] BPT diagram. SF regions are colour-coded in blue, LIER in orange, Seyfert like in red, (7) velocity field of the stars, (8) velocity field of the gas. For all maps, the colour bar increases from blue to red and the values corresponding to the minimum and maximum of the colour-bars are annotated on the top right corner of each map. The average PSF for the MaNGA data is shown in the bottom right corner of the maps.

and BPT classification (blue corresponding to SF, orange to LIER and red to Sy-like regions).

In this work, we make use of 583 galaxies selected from the sample described in Paper I. In particular, we exclude Seyfert galaxies, mergers and galaxies with an ambiguous classification and classify all the remaining galaxies as described in Paper I, i.e.:

(i) *Line-less galaxies*: no detected line emission (average EW(Hα) <1.0 Å within 1 R_e).

(ii) *Extended LIER galaxies (eLIER)*: galaxies dominated by LIER emission at all radii where emission lines are detected. No evidence for any SF regions.

(iii) *Central LIER galaxies (cLIER)*: galaxies where LIER emission is resolved and located in the central regions, while ionization from star formation dominates at larger galactocentric distances.

(iv) *Star -forming galaxies (SF)*: galaxies dominated by star formation in the central regions and at all radii within the galaxy disc.

Downloaded from https://academic.oup.com/mnras/article/466/3/2570/2666397 by INAF Trieste (Osservatorio Astronomico di Trieste) user on 25 November 2020

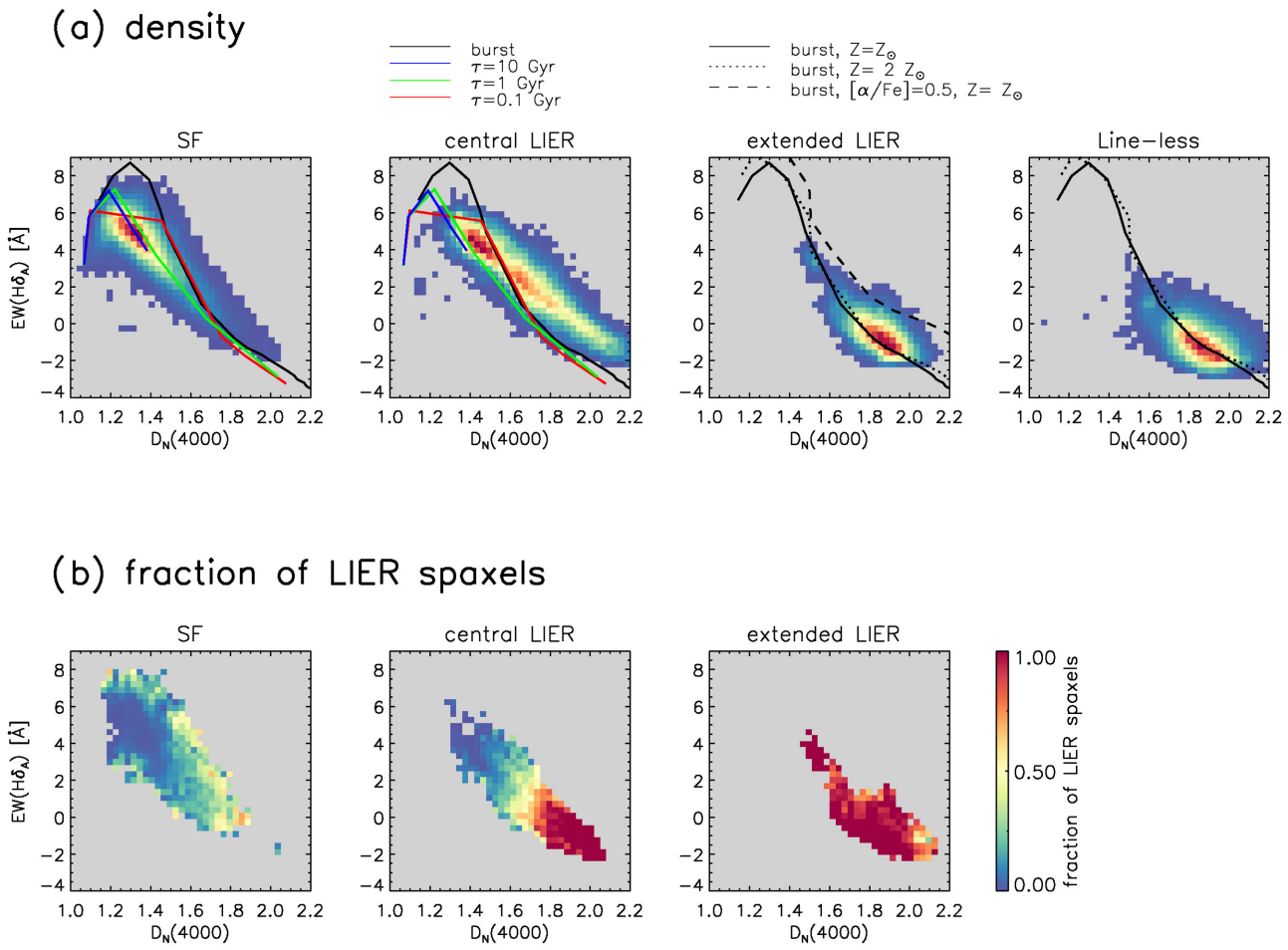


Figure 2. (a) Density plot in the $D_N(4000)$ versus EW($H\delta_A$) plane for spaxels in the different galaxy classes (SF, cLIER, eLIER and line-less) defined in this work. Different burst and continuous SFR models based on Maraston & Stromback (2011) stellar population models are overplotted (details in the legend). (b) Same as (a) but with the colour-coding reflecting the fraction of spaxels classified as LIER in each region of the $D_N(4000)$ versus EW($H\delta_A$) plane.

As discussed in Paper I, other 'ionization morphologies' are extremely rare. For example, we find no galaxy with a line-less bulge and a SF disc. The 583 galaxies used in this paper subdivide in the classes above as follows: 314 SF, 57 cLIER, 61 eLIER and 151 line-less.

3.2 From nebular lines to stellar indices: tracing star formation and quiescence

The realization that LIER emission is not related to nuclear activity, but simply a consequence of presence of a diffuse UV background due to evolved stellar populations, leads us to reconsider the conventional definition of quiescence as absence of nebular line emission. Namely, both LIER and line-less regions [EW($H\alpha$) $<$ 1 Å] can be defined as 'quiescent' (or 'passive'), to highlight the fact that they do not host current star formation as traced by the dominant component of line emission.

An alternative definition of quiescence may rely on probes of star formation on longer time-scales, such as the so-called 4000 Å break [$D_N(4000)$, Balogh et al. 1999] that is a sensitive tracer of the age of the stellar population. More specifically, while $D_N(4000)$ is also sensitive to metallicity effects (for stellar population older than 1 Gyr), the combination of $D_N(4000)$ and the stellar index EW($H\delta_A$) is less sensitive to the effect of metallicity and has been used in the literature as a probe for the galaxy's star formation history (e.g. Kauffmann et al. 2003a,b; Li et al. 2015). In Paper I, we have demonstrated that a selection on $D_N(4000)$ or EW($H\alpha$) is generally equivalent to our emission-line-based classification, as LIERs are characterized by the absence of young stars.

In Fig. 2a), we plot the MaNGA spaxels divided by galaxy class (SF, cLIER, eLIER and line-less) in the $D_N(4000)$ versus EW($H\delta_A$) plane. Model tracks, based on Maraston & Stromback (2011) stellar population models, are shown for a burst of star formation (with solar metallicity, solid black line in all panels) and three models with continuous, exponentially declining star formation (where the SFR decline time-scale, τ, is varied in the range 0.1–10 Gyr). Except for the increase in EW($H\delta_A$) observed in the burst model at young ages ($<$1 Gyr), stellar population age increases going from top-left to bottom-right. The black dotted models in the eLIER and line-less panels correspond to a burst of twice solar metallicity, and confirm that metallicity does not substantially affect the position in the $D_N(4000)$ versus EW($H\delta_A$). In all panels, the burst model defines an envelope in $D_N(4000)$-EW($H\delta_A$), with continuous SFR models occupying regions at lower $D_N(4000)$ for a fixed EW($H\delta_A$) value.

Continuous star formation models are an excellent representation of the data for SF galaxies, with the model with $\tau = 10$ Gyr passing through the locus of the data. The data for cLIERs is bimodal in the $D_N(4000)$ versus EW($H\delta_A$) plane, spanning the full range of stellar

Downloaded from https://academic.oup.com/mnras/article/466/3/2570/2666397 by INAF Trieste (Osservatorio Astronomico di Trieste) user on 25 November 2020

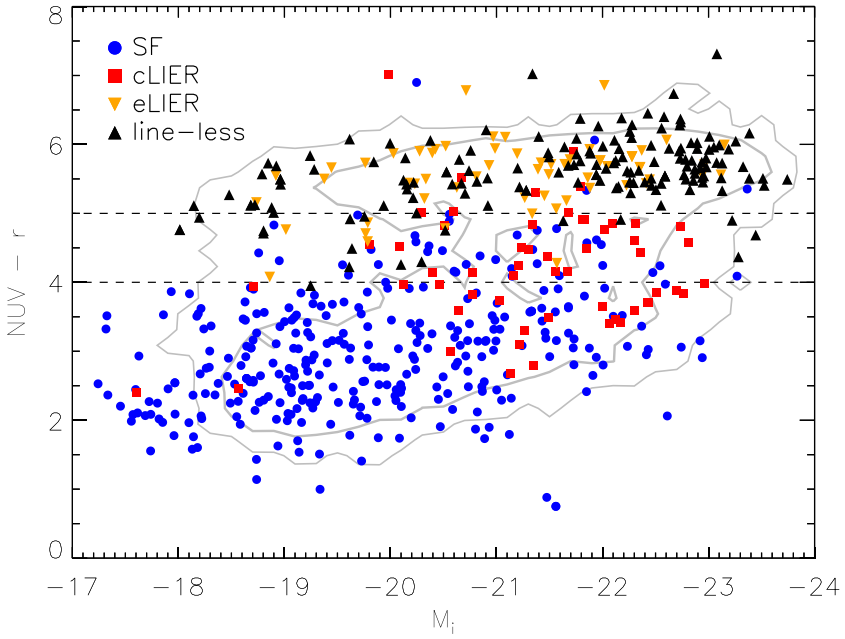


Figure 3. MaNGA galaxies in the $NUV - r$ versus M_i (colour-magnitude) diagram. Galaxies are divided according the emission-line-based classification introduced in Paper I (see also Section 2 of this work). Contours represent galaxy density in the MaNGA parent sample, while dashed lines provide a simple division between the red sequence ($NUV - r > 5$), green valley ($4 < NUV - r < 5$) and blue cloud ($NUV - r < 4$). The green valley is preferentially occupied by cLIER galaxies, while eLIER and line-less galaxies are mostly found on the red sequence ($NUV - r > 5$).

ages. The peak at $D_N(4000) \sim 1.4$ is well fitted by continuous SFR models with a decline time-scale of several Gyr. However, the second peak [$D_N(4000) \sim 1.7$] and the high-$D_N(4000)$ tail of the distribution is harder to fit with the available models because it lies above the burst model track. Dust can have an effect on the computed indices, especially $D_N(4000)$, and contribute to resolving the observed discrepancy.

The stellar populations of eLIERs and line-less galaxies are indistinguishable in the $D_N(4000)$–EW($H\delta_A$) plane and are well fitted by the burst model at old (>10 Gyr) ages. While the locus of the data does not require significantly α-enhanced stellar populations, α-enhancement can successfully explain the observed spread to higher EW($H\delta_A$) at fixed $D_N(4000)$ (dashed model track in eLIER panel, Thomas, Maraston & Korn 2004; Thomas, Maraston & Johansson 2011).

In Fig. 2(b), we show the same plot, but colour-coded by the fraction of spaxels classified as LIER across the $D_N(4000)$ versus EW($H\delta_A$) plane. The results demonstrate the strong correspondence between LIERs and old stellar populations, with cLIERs showing a transition from LIER-dominated central regions to SF-dominated outskirts.

The tight relation between line emission and stellar populations leads us to further investigate the emission-line based galaxy classification in the context of the broader physical properties of galaxies. In this work, we wish to address the question of how emission-line-based galaxy categories (SF, cLIER, cLIER and line-less) fit within the overall galaxy bimodality in terms of their fundamental properties (colours/morphology/kinematics). For example, can we interpret the SF, cLIER, eLIER and line-less galaxies sequence of increasing 'quiescence' as an evolutionary sequence? Where does the gas in eLIER galaxies come from and what makes these galaxies different from line-less galaxies? Here, we attempt to answer these questions by taking advantage of both the MaNGA data and legacy SDSS photometry and spectroscopy.

4 LIER GALAXIES WITHIN THE BIMODAL GALAXY POPULATION

4.1 Integrated colours and star formation rates

The physical origin of the colour bimodality in the galaxy population lies in the idea of using galaxy colour as 'clocks'. Both UV and blue colours evolve quickly once O and B stars disappear from the galaxy spectrum. In particular, NUV emission declines more slowly than Hα ($\sim 10^6$–10^7 yr), but faster than blue optical continuum ($\sim 10^9$ yr), making UV-optical colours a sensitive probe to the fading of young stellar populations.

Fig. 3 shows the $NUV - r$ versus M_i (i-band absolute magnitude) diagram for the current MaNGA sample, with galaxies subdivided according to the emission-line-based classification scheme introduced in this work. We observe that SF galaxies constitute the vast majority of the blue cloud ($NUV - r < 4$), while line-less and eLIER galaxies are concentrated on the red sequence ($NUV - r > 5$). The most striking feature of Fig. 3 is that a large fraction of cLIER galaxies (~40 per cent) are found in the green valley ($4 < NUV - r < 5$), with the remaining ones also lying at intermediate UV-optical colours (the mean $NUV - r$ for cLIERs is 4. 1 with a standard deviation of 1.0 mag). The prevalence of cLIER galaxies in the green valley is not surprising, since the integrated colours are affected by both the light from the red, old, LIER-like central regions and light from the blue, SF disc, thus generating the observed intermediate integrated colours. The separation of cLIER galaxies from the blue cloud is less evident when using optical colours (for example $u - r$ or $g - r$ instead of $NUV - r$). Indeed, using $g - i$ colours, cLIER galaxies are consistent with lying on the red sequence, and have equivalent colour to eLIERs and line-less galaxies. Further details on the UV-optical colours of different galaxy classes are summarized in Table 1.

Fig. 4 presents an even more striking illustration of the transition nature of cLIER galaxies, by representing the MaNGA galaxies

Downloaded from https://academic.oup.com/mnras/article/466/3/2570/2666397 by INAF Trieste (Osservatorio Astronomico di Trieste) user on 25 November 2020

Table 1. Classification statistics of emission-line galaxies in the $NUV - r$ colour–magnitude diagram and mean (± standard deviation) for selected UV and optical colours. Appropriate volume weights have been applied to correct for the MaNGA selection function.

Galaxy class	Blue cloud $NUV - r < 4$	Green valley $4 < NUV - r < 5$	Red sequence $NUV - r > 5$	$NUV - r$ $\mu \pm \sigma$	$u - r$ $\mu \pm \sigma$	$g - r$ $\mu \pm \sigma$
SF	92%	7%	1%	2.8 ± 0.8	1.6 ± 0.4	0.55 ± 0.16
cLIER	48%	39%	13%	4.1 ± 1.0	2.2 ± 0.3	0.74 ± 0.10
eLIER	0	19%	81%	5.4 ± 0.6	2.5 ± 0.2	0.78 ± 0.09
line-less	1%	14%	85%	5.5 ± 0.7	2.4 ± 0.2	0.76 ± 0.09

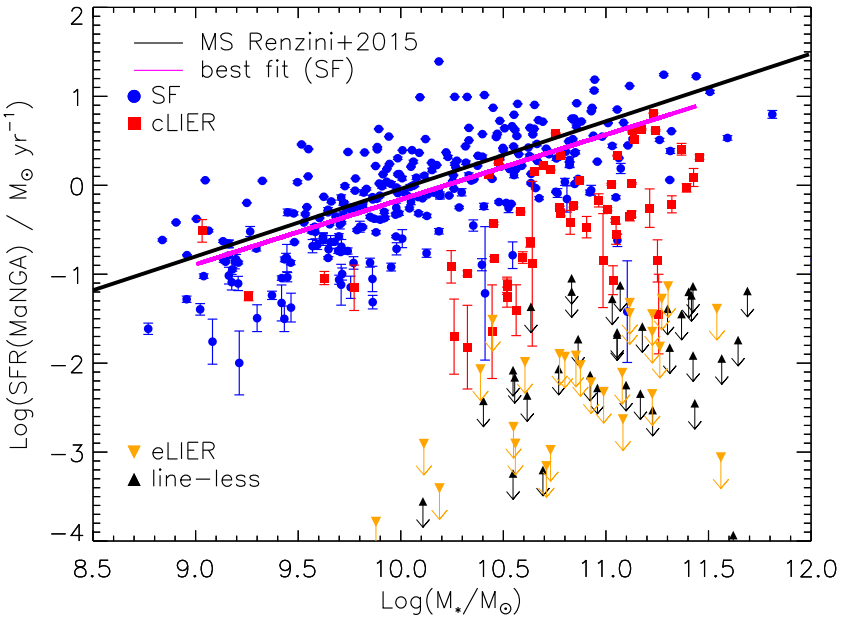


Figure 4. The SFR–$M_\star$ plane for MaNGA galaxies. The SFR from the extinction-corrected Hα flux by summing the flux in spaxels classified as SF. The black line represent the 'main sequence' for SF galaxies from legacy SDSS spectroscopy (Renzini & Peng 2015). The magenta line represents the best-fitting 'main sequence' using the SF galaxies in the MaNGA sample.

in the SFR–$M_\star$ plane. The SFR is calculated from the extinction-corrected Hα flux within the MaNGA bundle and using the Kennicutt (1998) conversion factor. The procedure used to correct the SFR for LIER emission is based on the assumption that the total Hα flux can be decomposed into a contribution from star formation (with line ratios typical of SF regions) and from LIERs/diffuse ionized gas (with line ratios typical of LIERs). The details of the correction procedure are presented in Appendix A. This procedure generates SFR estimates that are on average indistinguishable from the SFR computed using only the spaxels classified as SF using the [S II] BPT diagram. For LIER regions, only a small fraction of the Hα flux can be attributed to underlying star formation, and we thus consider the SFR for eLIER and line-less galaxies as upper limits. We do not apply any aperture correction to the MaNGA-derived SFR. Errors on the SFR are estimated by propagating the uncertainties in the flux and extinction correction.

Fig. 4 demonstrates that SF galaxies lie on the 'main sequence' (Brinchmann et al. 2004; Salim et al. 2007; Peng et al. 2010; Renzini & Peng 2015) while the cLIER galaxies lie systematically below it, although above the passive galaxy population, consisting of eLIERs and line-less galaxies. For reference we plot the 'main sequence' at $z \sim 0$ from Renzini & Peng (2015) (black solid line in Fig. 4), obtained from legacy SDSS spectroscopy, and the best-fitting line to the SF galaxy population using the current MaNGA sample [with $9 < \log(M_\star/M_\odot) < 11.5$, magenta line in Fig. 4], given by

$$\log\left(\frac{\mathrm{SFR}}{M_\odot\ \mathrm{yr}^{-1}}\right) = -7.5\ \pm 0.2 + (0.73\ \pm 0.02)\ \log\left(\frac{M_\star}{M_\odot}\right) \quad (1)$$

Considering the differences in sample selection and methodology for calculating stellar mass and SFR, results from legacy SDSS are in excellent agreement with the MaNGA result presented here. At a fixed stellar mass, cLIER galaxies lie on average 0.8 dex below the main sequence defined by the SF population, although they actually spread across the entire green valley with large scatter.

Summarizing, the key results from this section are the following: (1) eLIER and quiescent line-less galaxies are indistinguishable in terms of colours; (2) most green valley galaxies are not such because of dust reddening or globally intermediate stellar populations, but are associated with galaxies (cLIERs) in which quiescent (non-SF) central regions co-exist with outer star formation. These galaxies lie in the transition region between the star formation main sequence and quiescent galaxies.

4.2 Morphological type

The traditional morphological dichotomy between early-type (ETG, E and S0) and late-type galaxies (LTG, spirals), as implemented in the revised Hubble classification (Sandage 1961), is based on

Downloaded from https://academic.oup.com/mnras/article/466/3/2570/2666397 by INAF Trieste (Osservatorio Astronomico di Trieste) user on 25 November 2020

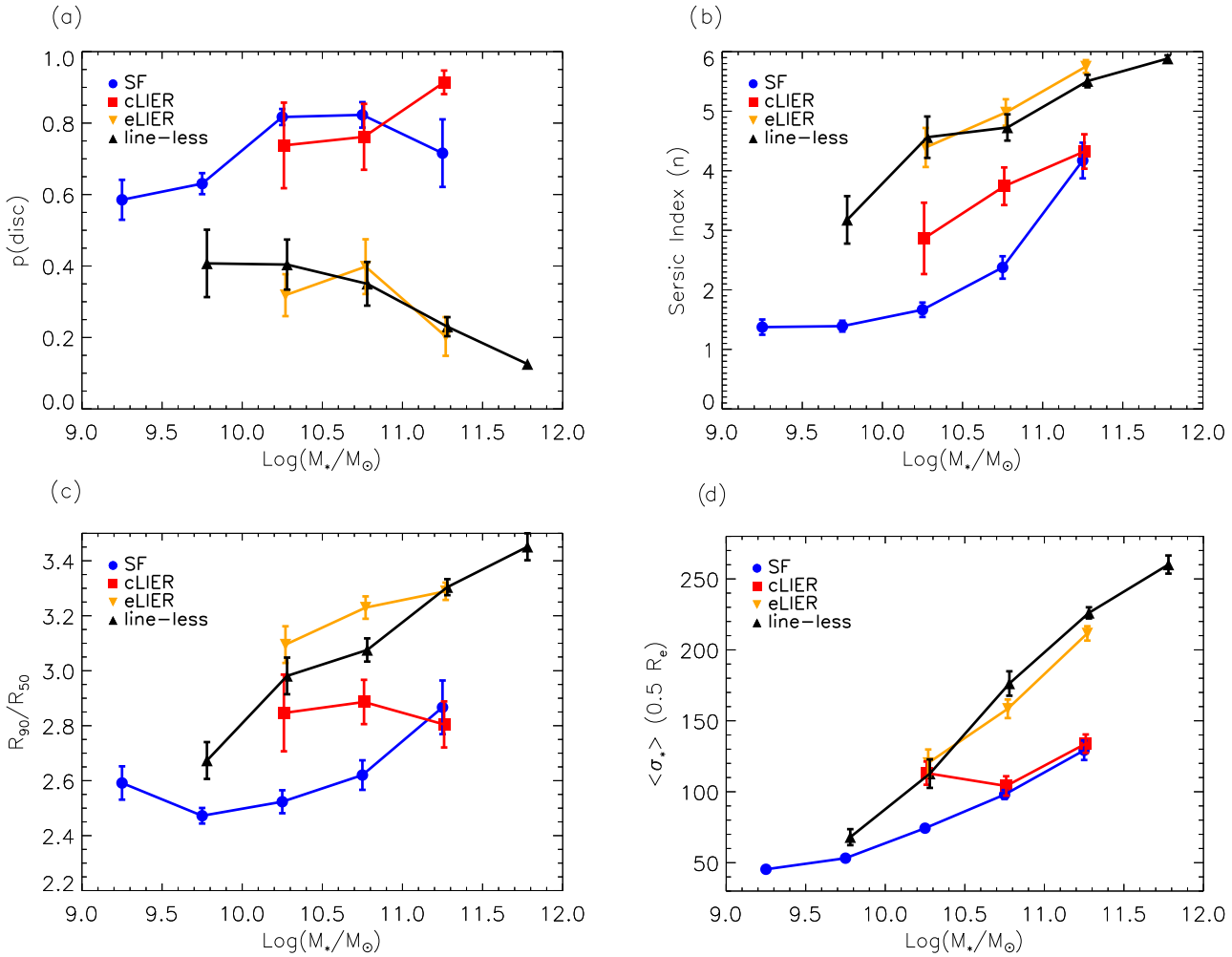


Figure 5. (a) Average disc vote fraction from Galaxy Zoo 2 (Willett et al. 2013) in bins of stellar mass for MaNGA galaxies of different classes. The vote fraction can be interpreted as a probability and has been statistically de-biased to account for the increasing difficulty of detecting fainter morphological features at higher redshift following Willett et al. (2013). (b), (c) Average Sérsic index and concentration (defined as R_{90}/R_{50}, where R are Petrosian radii) in bins of stellar mass. Sérsic parameters and Petrosian radii are obtained from the NSA (Blanton et al. 2011) and are based on legacy SDSS r-band imaging. (d) Average stellar velocity dispersion within 0.5 R_e in bins of stellar mass. Velocity dispersions are calculated from the MaNGA data and R_e is the Sérsic r-band effective radius from the NSA catalogue.

the presence or absence respectively of spirals arms and/or dust lanes when galaxies are seen edge on. Subsequent revisions to this classification, including recent advanced made possible by IFS observations, have conclusively demonstrated that a large fraction of ETG contain discs seen at a variety of inclinations (dubbed as 'fast rotators' by the ATLAS^{3D} project). Only the most massive end of the ETG population is populated by true dispersion dominated systems ('slow rotators'), with very little ordered angular momentum (Emsellem et al. 2007, 2011; Cappellari et al. 2011a). Extensions to higher redshift (Bundy et al. 2010) seem to confirm this general picture.

Visual morphological classifications from the Galaxy Zoo 2 project (Lintott et al. 2008; Willett et al. 2013), based on legacy SDSS imaging, were used to subdivide MaNGA galaxies into ETG and LTG. In particular, we make use of the detailed classification from Galaxy Zoo 2, which asked its volunteer citizen scientists to identify several morphological features (spirals, bars etc.) in SDSS three-colour image cutouts. Individual classifications are processed as detailed in Willett et al. (2013) and statistically 'de-biased' to take into account the fact that is it harder to identify fine morphological features for smaller, fainter galaxies. The nature of the Galaxy Zoo vote fractions means that they can be interpreted as conditional probabilities, although one needs to take into account that not all parameters are estimated for all galaxies, given the decision tree nature of the Galaxy Zoo 2 classifications. Vote fractions for certain questions (hence features) are only computed if previous questions in the decision tree are 'well answered' (as detailed in Willett et al. 2013, section 3.3 and table 3).

In Fig. 5, we plot the median trends in bins of stellar mass for the de-biased probability of the presence of disc or other feature[2] in our MaNGA galaxy sample, classified according to the emission-line-based classification. In order to study trends as a function of stellar mass we correct for the effect of the MaNGA selection function. The error bars represent the error on the mean in each mass bin. The results from the Galaxy Zoo 2 classifications demonstrate that eLIER and line-less galaxies have mutually consistent morphologies and

[2] Task 1 in Galaxy Zoo 2, addressing the question: *Is the galaxy simply smooth and rounded, with no sign of a disc?*

Downloaded from https://academic.oup.com/mnras/article/466/3/2570/2666397 by INAF Trieste (Osservatorio Astronomico di Trieste) user on 25 November 2020

are visually classified as ETGs. SF and cLIER galaxies, on the other hand, also have mutually consistent disc fractions and are consistent with being LTGs. Although outliers are present in either direction (SF galaxies with no disc features or line-less galaxies classified as discs), these do not dominate the sample averaged trends.

Interestingly, previous work based on Galaxy Zoo has highlighted the fact that when galaxies are classified into a red sequence and blue cloud using optical colours, the red sequence host a substantial fraction of red ('anemic') spirals (Bamford et al. 2009; Masters et al. 2010). cLIER galaxies, because of their substantially redder optical colours than the mean of the blue cloud (see Table 1) and their disc-like morphology, may appear as 'red spirals' in integrated colours. This class of galaxies represents a natural link between normal spirals and lenticular (S0) galaxies, as suggested in the revised 'trident' morphological classification van den Bergh (1976) and further updated by Cappellari et al. (2011a).

Further support towards a relation between the anemic spiral class and cLIERs is given by the fact that anemic spirals in single-fibre spectroscopy (Masters et al. 2010) are often classified as LIERs, have lower EW(Hα) than SF galaxies, present older mean stellar ages (Tojeiro et al. 2013) and are found to be an insignificant fraction of the total spiral population for $M_\star < 10^{10}\,\mathrm{M}_\odot$ (Wolf et al. 2009) while representing as much as 40 per cent of the spiral population at the highest masses ($M_\star > 10^{10.8}\,\mathrm{M}_\odot$, Masters et al. 2010).

4.3 The importance of the bulge

Morphological features such as spiral arms and bars only capture one aspect of the complex problem of morphological classification of galaxies. Another characteristic generally associated with the study of galaxy morphology is the presence and importance of a central spheroidal component (the bulge). Unfortunately, although parametric bulge-disc decomposition is a well-established technique, studies based on photometry alone are limited by the well-known intrinsic degeneracies in the method (Rybicki 1987; Gerhard & Binney 1996). Although potentially even more biased, 'cheaper' proxies such as the 'concentration' index (here defined as $C = R_{90}/R_{50}$ where R are Petrosian radii) or a galaxy-averaged Sérsic index have often been used on large photometric samples to provide an observationally more well-defined estimate of the importance of the bulge/spheroidal component. As a complement to these photometric indicators we also study the central stellar velocity dispersion extracted from the MaNGA data, which is a direct proxy for the depth of the bulge gravitational potential.

In this context, it is important to note that, if the bulge is defined kinematically, the classical lenticular (S0) morphological class is found to span a wide range in bulge fraction, forming a sequence essentially parallel to the classical increase in bulge fraction from Sc to Sa for LTGs (Cappellari et al. 2011b; Krajnović et al. 2013; Cappellari 2016). Indeed, it is arguable whether the traditional S0 morphological classification is in itself meaningful, as IFS surveys have demonstrated that the photometry alone is a very poor predictor of the degree of rotational support for ETG, with S0 likely to be classified as classical dispersion dominated ellipticals when viewed at low inclinations (e.g. Emsellem et al. 2011).

In Fig. 5(b–d), we show the average Sérsic index, concentration and stellar velocity dispersion within 0.5 R_e ($\langle\sigma_\star\rangle$) as a function of galaxy class in bins of stellar mass. In each bin, an average value is plotted only if there are more than four galaxies in the bin. As expected from their early-type morphology, both line-less and eLIER galaxies show higher Sérsic indices, concentrations and $\langle\sigma_\star\rangle$ than cLIER and SF galaxies in all stellar mass bins. cLIERs have Sérsic indices, concentrations and $\langle\sigma_\star\rangle$ intermediate between eLIER/line-less and SF galaxies, consistent with the idea of being the subset of disc-dominated galaxies with largest bulge component at each stellar mass. For purely SF galaxies Sérsic index, concentration and $\langle\sigma_\star\rangle$ all increase as a function of mass, matching those of cLIER galaxies in the mass bin $11.0 < \log(M_\star/\mathrm{M}_\odot) < 11.5$. Note that when using the central velocity dispersion as a tracer of the bulge potential we recover the same overall trends as for pure photometric tracers like Sérsic index and concentration, thus confirming that our results are not dominated by the uncertainty in the photometry.

5 KINEMATIC MISALIGNMENT

Kinematic decoupling between the gaseous and stellar components has been observed to be common in local ETGs (Bertola et al. 1999; Sarzi et al. 2006; Davis et al. 2011), with hints of this behaviour being already present at high redshift (Wisnioski et al. 2015). The distribution of misalignments between the gas and stars is a direct probe of the origin of the gas in ETG. Theoretically, a newly formed gas disc is predicted to precess due to the effect of the gravitational potential of the stars, with gas precessing faster at smaller radii, where the torque is larger. Cloud–cloud collisions will also work to realign the differently precessing gas rings, and the system will eventually settle into a configuration where the gas and stellar components are either aligned or misaligned by 180°. The relaxation time for this process was initially predicted to be of the order of dynamical time (Tohline & Durisen 1982; Lake & Norman 1983), however recent work based on hydrodynamics in the cosmological framework has highlighted that misalignments might persist on much longer (several Gyr) time-scales (van de Voort et al. 2015), mostly because of the effect of continuous cosmological accretion. This longer relaxation time-scale also provides a better fit to the misalignment distributions observed in the literature (Davis & Bureau 2016). For weakly triaxial systems stable gaseous orbits are allowed both in the plane containing the long and intermediate axes and the plane of the short and intermediate axis (Franx, Illingworth & de Zeeuw 1991). If the origin of the gas is external therefore the distribution of the gas–stars kinematic misalignment should display three peaks, respectively at 0, 90, 180°, with the peak around 90° being weaker and scaling with the degree of triaxiality.

In this section, we derive the kinematic position angle (PA) of both gas and stars following the procedure in Krajnovic et al. (2006). In short, having fixed the kinematical centre to the photometric one, the algorithm constructs a bi-antisymmetric version of the velocity field and compares it with the observed velocity field. The resulting PA is thus only representative of the axis of symmetry of the velocity field and the measurement does not imply that the galaxy is best fitted with a thin disc model. In our sample four galaxies present particularly complex gaseous kinematics with no obvious symmetry axis and have been excluded from the following analysis. Two of these galaxies show approaching/trailing features while other two show evidence for extreme changes in the direction of rotation of the gas (MaNGA-ID `1-38167`, `1-274663`).

The remaining eLIER galaxies in our sample display a wide range of gas velocity field patterns. While some galaxies are consistent with a gaseous disc rotation, in other systems the velocity field appears disturbed. Overall, the large majority of galaxies in this class show coherent velocity shear patterns, showing both red and blue-shifted emission. However, these gas flows are not always associated with large-scale rotation. For example, in Cheung et al. (2016) we propose a biconical outflow model for an eLIER galaxy (MaNGA-ID `1-217022`) that has recently been subject to a

Downloaded from https://academic.oup.com/mnras/article/466/3/2570/2666397 by INAF Trieste (Osservatorio Astronomico di Trieste) user on 25 November 2020

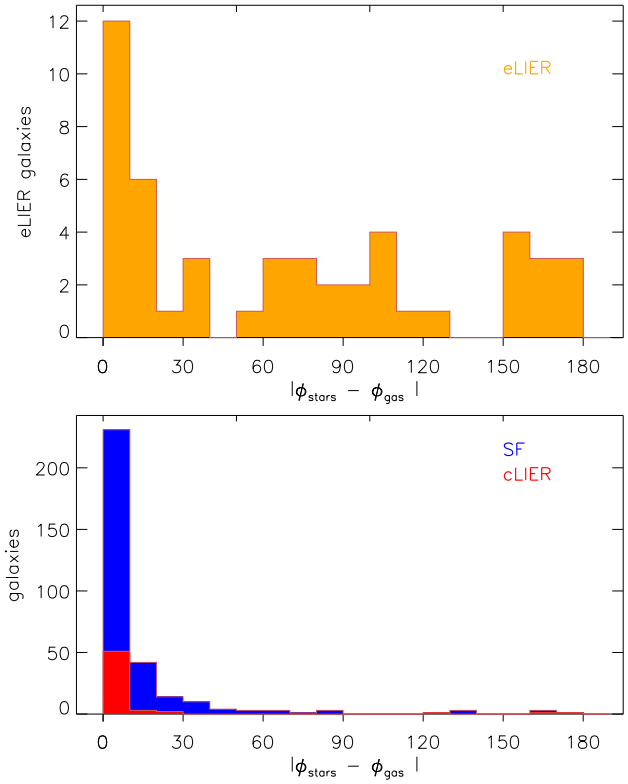


Figure 6. Histograms of the distribution of kinematic misalignments between the position angle of the major axis of the stellar component and of the ionized gas for the eLIER galaxies (top) and SF and cLIER galaxies (bottom) in the current MaNGA sample.

minor merger event (as demonstrated by the presence of a nearby companion and the detection of neutral gas via the NaD absorption feature).

The observed distribution of stars–gas misalignment for the eLIER galaxies in our sample is shown in Fig. 6, with 30 out of 49 galaxies having misalignments larger than 30°. Making the appropriate volume corrections, necessary in order to take into account the MaNGA selection function, we infer that 65 ± 7 per cent of eLIERs are misaligned with $|\phi_{stars} - \phi_{gas}| > 30°$. This number is significantly larger from that inferred by the SAURON and ATLAS^{3D} surveys (Sarzi et al. 2006; Davis et al. 2011). However, both surveys adopt a pure morphological selection, thus including galaxies with residual star formation into their sample, which would not be classified as eLIERs. Galaxies with detectable star formation (SF and cLIERs) have a misalignment distribution strongly peaked at zero (Fig. 6, bottom panel, only 11 ± 2 per cent with $|\phi_{stars} - \phi_{gas}| > 30°$), thus a small contamination from SF or cLIER galaxies can bring our result in line with previous work. Moreover, our results confirm the theoretical prediction for the case of external accretion, as the observed distribution of misalignments for eLIERs is peaked at 0, 90 and 180°.

In absence of internal processes (i.e. stellar mass-loss), the misalignment histogram is predicted to be *symmetric* around 90° (Davis & Bureau 2016). Making the assumption of isotropic accretion and long relaxation times, one would naively expect 150/180 ∼ 83 per cent of galaxies to have misalignments larger than 30°. The presence of a stronger peak at zero and the fact that the number of misaligned galaxies is lower than a naive estimate for isotropic accretion implies that internal processes are also likely to play a role, although secondary, in shaping the observed misalignment distribution. In particular, stellar mass-loss will not only inject into the ISM some amount of gas sharing the same kinematic properties as the parent stars, but would also create additional torque on the accreted misaligned gas and contribute to realign it with the stellar kinematic field. Both effects would contribute to increase the fraction of aligned galaxies.

6 THE EFFECT OF ENVIRONMENT

Fundamental properties of the bimodal galaxy population, including colour, SFR and passive fraction are found to depend both on stellar mass and environment (Blanton et al. 2005a; Baldry et al. 2006; Peng et al. 2010). Using data from legacy SDSS, it has been demonstrated that the change in EW(Hα) distribution as a function of environment is predominantly due to a change in the relative number of SF and passive galaxies (Balogh et al. 2004). If one restricts the study to SF galaxies, the EW(Hα) (or equivalently the specific SFR) is observed *not* to depend on environment, i.e. if a galaxy forms stars on the main sequence, environments does not effect its SFR (Peng et al. 2010), which is consistent with the finding that stellar population ages do not depend on environment (Thomas et al. 2010). However, passive galaxies with measurable EW of line emission (eLIERs in our classification) have long been associated with inefficiently accreting AGN (e.g. Kauffmann et al. 2003c; Kewley & Ellison 2008) and their role as red sequence galaxies with residual gas has not yet seen suitably discussed in the context of environmental studies.

In this work, we have highlighted the similarities of eLIER to lineless galaxies in terms of the stellar populations and morphological properties. Given these observed similarities, it is logical to ask whether environment plays a role in the presence or absence of line emission on the red sequence. Some evidence in this direction was reported by Sarzi et al. (2006), who found a small difference in the fraction of detected line emission between ETGs in the Virgo cluster compared to the field.

In order to address this question with a large sample of galaxies, in this section we make use of the MaNGA parent galaxy sample (Wake et al. in preparation), and study the emerging trends as a function of different environmental measures. We do not use the MaNGA data directly because the sample of LIER galaxies currently available is too small to reliably study environmental trends in several stellar mass bins. The MaNGA parent sample, on the other hand, includes all galaxies from the NSA catalogue that match the MaNGA target selection criteria (∼30 000 galaxies). We use legacy SDSS spectroscopy (Strauss et al. 2002), and make use of the line flux measurements from the MPA-JHU catalogue (Kauffmann et al. 2003c; Brinchmann et al. 2004; Tremonti et al. 2004) to compute the BPT classifications of each galaxy. In order to study trends as a function of stellar mass we correct for the effect of the MaNGA selection function.

In order to adapt the cLIER/eLIER distinction to single-fibre legacy SDSS, which does not cover the outer regions of galaxies, we make use of the integrated UV-optical colours, based on the findings in Section 4.1 above. We assume that both cLIERs and eLIERs would appear as LIER galaxies in single fibre spectroscopy. A galaxy appearing as LIER in single-fibre spectroscopy is classified as cLIER if it lies on the blue cloud or the green valley ($NUV - r < 5$) and eLIER if it lies on the red sequence ($NUV - r > 5$) using UV-optical colours. We make use of the MaNGA parent sample instead of the full legacy SDSS in an attempt to minimize

Downloaded from https://academic.oup.com/mnras/article/466/3/2570/2666397 by INAF Trieste (Osservatorio Astronomico di Trieste) user on 25 November 2020

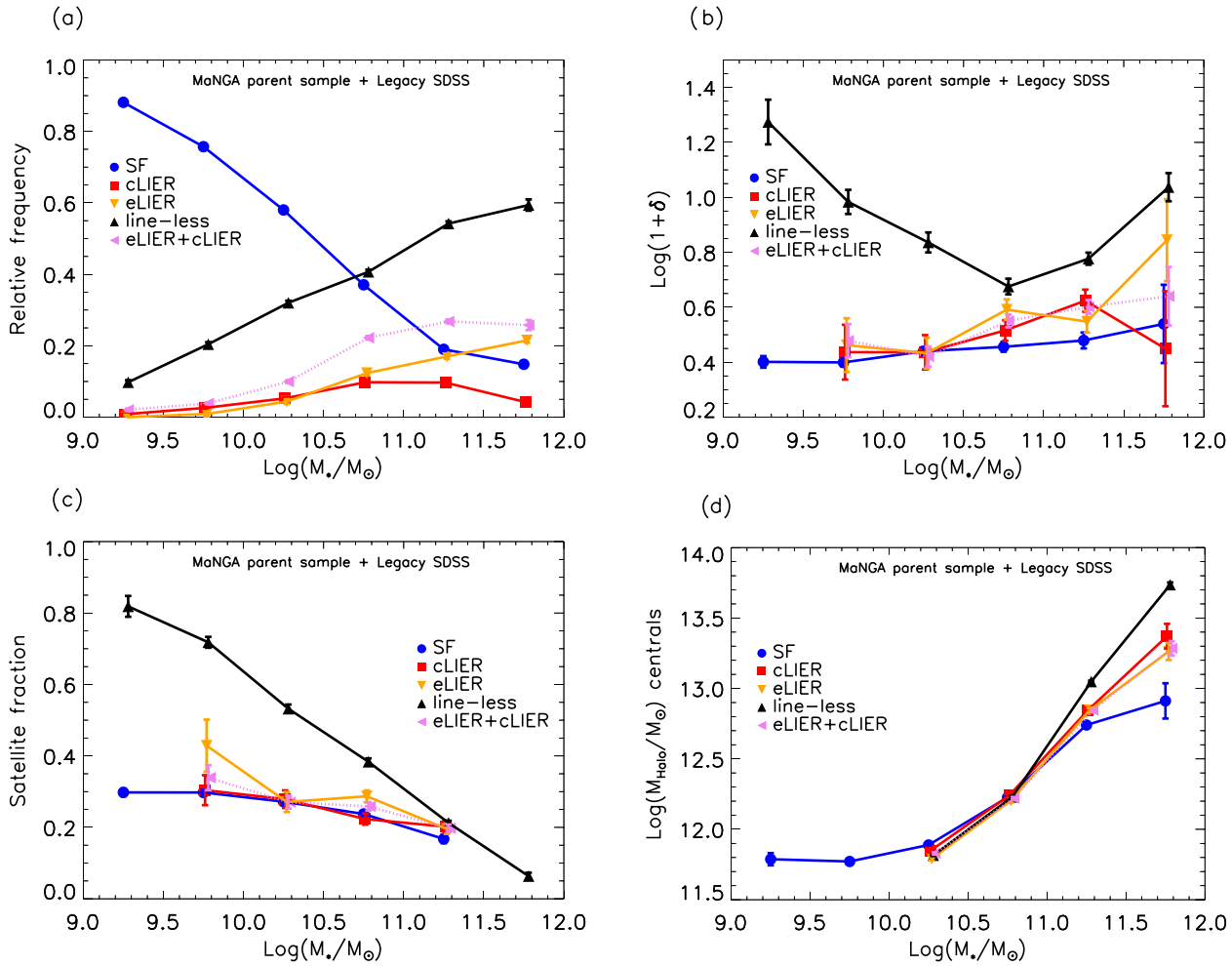


Figure 7. (a) The relative frequency of galaxies in different emission-line-based classes derived from the MaNGA parent catalogue and legacy SDSS spectroscopy in bins of stellar mass. (b) Average overdensity as a function of stellar mass for galaxies of different emission-line classes, based on the MaNGA parent catalogue and SDSS legacy spectroscopy. (c) Average fraction of galaxies classified as satellites in the Yang et al. (2007) group catalogue for each emission-line-based galaxy class as a function of stellar mass. The galaxy sample is taken from the MaNGA parent sample, complemented with SDSS legacy spectroscopy. (d) Average halo mass for galaxies classified as central in the Yang et al. (2007) group catalogue for each emission-line bases galaxy class as a function of stellar mass. The galaxy sample is taken from the MaNGA parent sample, complemented with SDSS legacy spectroscopy. In each plot, the error bar represents the error on the mean and only bins containing more than four galaxies are shown. The dotted line (eLIER+cLIER) refers to the union of both cLIER and eLIER classes.

the role of aperture effects in this classification, an effect that is otherwise difficult to quantify. According to Section 4.1, our mixed spectroscopic + photometric eLIER/cLIER distinction introduces a 19 per cent contamination for eLIERs and 13 per cent contamination for cLIERs. Similarly, in the attempt to replicate in the best possible way the MaNGA-based classification, galaxies with EW(Hα) < 1.0 Å within the 3 arcsec SDSS fibre are considered line-less. Seyfert AGN, as identified using the [S II] BPT diagram, are excluded from this analysis.

In Fig. 7(a), we show the fraction of galaxies in each class as a function of mass in the MaNGA parent sample. This figure is to be compared with the equivalent figure in Paper I (Fig. 6) for the MaNGA sample that is also used in this work. Qualitatively the mass trends for each class are similar, however some differences are also present. In particular, the classification based on legacy SDSS finds less LIER galaxies than in the MaNGA data, which might be due to residual aperture effects.

In order to study environmental effect, we make use of adaptive aperture environmental measure presented in Etherington & Thomas (2015). The cosmic density ρ field is calculated using a cylinder centred on each galaxy and with length of 1000 km s^{-1} and radius given by the distance to the fifth nearest neighbour more luminous than $M_r < -20.26$ (where M_r is the k-corrected r-band magnitude). The environment estimator is cast in terms of an overdensity [$\delta = (\rho - \rho_m)/\rho_m$] relative to the average density of tracer galaxies ρ_m and is most sensitive to scales around 2 Mpc (Etherington & Thomas 2015).

We further make use of the environmental information provided by the Yang et al. (2005, 2007) group catalogue. The catalogue is based on a halo-finding algorithm applied to the NYU-Value Added Catalogue (Blanton et al. 2005a), based on legacy SDSS DR7 data. Galaxies belonging to the same dark matter halo are defined to constitute a 'group' (where the term group is used here irrespective of the number of galaxies in the association). The most luminous galaxy in each group is defined to be the 'central', while the other galaxies in each group are defined to be 'satellites'. Note that, following this definition, centrals do not need to necessarily lie at the geometric centre of the dark matter halo. Several galaxies are

Downloaded from https://academic.oup.com/mnras/article/466/3/2570/2666397 by INAF Trieste (Osservatorio Astronomico di Trieste) user on 25 November 2020

assigned to haloes that contain no other galaxy within them; these galaxies are called centrals even though no satellites are detected in SDSS (although deeper observations might reveal their presence). The halo mass ($M_{\rm halo}$) is calculated for each group by Yang et al. (2007) considering the characteristic integrated luminosity (above some flux limit, and corrected for incompleteness) of the group members calibrated against the dark matter masses derived from models.

In Fig. 7(b) we show the mean environmental density as a function of stellar mass for each galaxy class (SF, cLIER, eLIER and line-less). The plot demonstrates that (1) At fixed stellar mass, line-less galaxies always live in denser environments than eLIER galaxies. The relative difference in environmental density between the two galaxy classes is large at both the lowest and highest stellar masses, with a minimum difference at $M_\star \sim 10^{10.5}$ M$_\odot$. (2) There is only a marginal difference in environmental density between SF galaxies and cLIER or eLIERs, with eLIERs living in marginally denser environments.

For the purpose of the study of line emission in the overall galaxy population, the most striking feature of Fig. 7(b) is the large difference in environmental density between eLIERs (i.e. red sequence galaxies with line emission) and line-less galaxies (i.e. red sequence galaxies with EW(Hα) < 1.0 Å). The legacy SDSS data demonstrate clearly that the lack of line emission on the red sequence is associated with higher environmental densities. We discuss the possible physical processes that could be responsible for this phenomenon in Section 7.2.

Fig. 7(c) demonstrates that line-less galaxies have a substantially higher satellite fraction than any other galaxies class at all stellar masses lower than $M_\star \sim 10^{11}$ M$_\odot$. Hence, the increase in the environmental density of line-less galaxies at low stellar masses is mostly driven by the fact that these galaxies are preferentially satellites.

At high stellar masses, on the other hand, line-less central galaxies have a higher mean halo mass than other galaxy classes (Fig. 7d). Higher mass haloes tend to have a higher number of satellites and also to be more strongly clustered, thus explaining the increase in environmental density at the high-mass end. The figure also shows that in the highest mass bin, SF galaxies reside in lower mass haloes than LIER galaxies (both eLIERs and cLIERs).

7 DISCUSSION: AN EVOLUTIONARY SCENARIO FOR LIERS

7.1 Inside-out quenching and the nature of cLIER galaxies

7.1.1 A slow quenching pathway for late-type galaxies

The properties of cLIERs are such that they can be considered objects in transition (in the process of being 'quenched') from the SF blue cloud towards the quiescent red sequence. The MaNGA spatially resolved data further demonstrate that star formation in these galaxies terminates from the inside out, with LIER emission appearing in the central regions, while star formation continues in the disc. The quenching process is not only evident via the lack of detected star formation in diagnostic diagrams, but also in the stellar population properties, as LIER emission is strongly correlated with old stellar populations (Section 3.2, also Paper I, section 7).

The process leading to the quenching of the central regions is likely to be gentle, since it does not involve a change in the overall morphology and kinematics of the galaxy, although it is associated with the presence of a large central spheroidal component. cLIER galaxies are thus consistent with the idea of a 'slow quenching mode' for LTGs (e.g. Schawinski et al. 2014; Smethurst et al. 2015). Different lines of evidence point towards the need of a such a 'slow quenching' pathway for LTGs associated with the increasing importance of the bulge component. Cappellari et al. (2013), for example, argue that the quenching process involved in the production of fast rotator ETGs needs to increase the bulge size, while at the same time removing the gas reservoir and/or shutting down star formation and maintaining the flatness of the disc at large radii. At higher redshift Bell et al. (2012) and Bundy et al. (2010) argue for a similar slow quenching pathway initiated by gradual changes in internal structure.

A possible quenching mechanism, much discussed in the literature (e.g. Wake et al. 2012; Bluck et al. 2014), assumes the higher central spheroidal masses to be directly connected to the cause of galaxy starvation via AGN radio-mode feedback. Indeed, larger bulge/spheroid masses imply larger black hole masses, hence higher capability of halo heating through radio-mode episodes (Heckman & Best 2014), which in turn may result into lack of gas cooling on to the host galaxy. While the inclusion of AGN radio-mode feedback in galaxy formation models has proven to be able to successfully solve a number of longstanding problems, direct evidence for this feedback mode in galaxies with $M_\star \sim 10^{10}$ M$_\odot$ remains lacking. It may be natural to assume that this feedback mode, generally predicted to be important in much more massive haloes (clusters, e.g. Fabian 2012) would equally affect lower mass haloes. However, other alternatives sharing the same scaling relation cannot be ruled out.

The interruption of the inflow of cold gas on to the galaxy ('strangulation'), due to either heating of the gas in the halo or via halo mass shock heating, can lead to an inside-out quenching signature, assuming that the remaining cold gas is consumed more quickly in the central regions of galaxies. As illustrated by Leroy et al. (2008) the efficiency of star formation (i.e. the number of stars formed per unit gas mass) is not constant across galaxy discs, but is observed to steadily decrease with galactocentric distance, thus making this scenario a viable option.

7.1.2 Secular processes and bulge growth

While a gas exhaustion scenario naturally produces slow, inside-out quenching, the simple strangulation scenario does not directly address the larger bulge components observed in cLIER galaxies compared to SF galaxies of the same stellar mass (unless one makes the additional assumption that bulge mass is driving the heating of the halo via radio-mode feedback).

Alternatively, the larger bulge masses, together with the implied slow time-scale for the quenching process, may argue in favour of secular processes (i.e. mechanisms internal to the galaxies) playing a role in the quenching process in cLIERs. Bars, for example, tend to funnel gas towards the galactic central regions, thus contributing to the formation of (pseudo)bulges (Kormendy et al. 2010; Cheung et al. 2013; Simmons et al. 2013). Moreover, simulations show that the torques and stresses created by both bars and bulges on the cold gas component can lead to lower star formation efficiency, especially in the regions swept up by the bar (Emsellem et al. 2015; Fanali et al. 2015). Indeed, bar fraction is known to correlate with the galaxy's stellar mass, colour and specific SFR (Nair & Abraham 2010; Masters et al. 2011), in the sense of redder and more massive, lower specific SFR discs having higher bar fraction. Moreover, bar fraction is observed to be higher in H I poor galaxies (Masters et al. 2012), although no similar investigation of

Downloaded from https://academic.oup.com/mnras/article/466/3/2570/2666397 by INAF Trieste (Osservatorio Astronomico di Trieste) user on 25 November 2020

the molecular gas content of a large sample of barred and unbarred galaxies has been possible to date (see Saintonge et al. 2012 for the largest sample to date).

Using the current MaNGA sample, for galaxies with $\log(M_\star/\mathrm{M}_\odot) > 10$ the bar fraction (defined as disc galaxies with $p_{\mathrm{bar}} > 0.3$ from Galaxy Zoo 2) is 32 ± 5 per cent for the SF discs, and 41 ± 11 per cent for the cLIERs. We thus conclude that the difference in bar fraction between the two classes is not significant with the current sample size, and a larger sample is needed to observationally test the relative occurrence of bars in SF galaxies are cLIERs.

Models predict that disc instabilities represent the dominant contribution to the formation of bulges in massive galaxies ($M_\star > 10^{10}\,\mathrm{M}_\odot$, De Lucia et al. 2011). Disc stability can be parametrized in terms of the stability parameter (Q, Toomre 1964), which in the case of gas+stars systems can be extended to include the two components (Jog & Solomon 1984; Elmegreen 1995; Martig et al. 2009; Romeo & Wiegert 2011). The presence of a significant bulge goes towards increasing the stability of a cold gas disc to gravitational collapse. Indeed, results from the COLD-GASS survey (Saintonge et al. 2011) demonstrate that galaxies with significant bulges have lower star formation efficiencies (Saintonge et al. 2012). Spatially resolved observations of the gas component for the MaNGA sample would be crucial in testing the role of the bulge in driving the star formation efficiency in different galaxy classes.

Star formation efficiency for cold gas is found to be systematically lower in ellipticals (Martig et al. 2013; Davis et al. 2014) and in the bulge of our own Galaxy (Longmore et al. 2013). Therefore, the absence of the star formation in the central regions of cLIERs could be due to a significantly lower star formation efficiency, even in presence of a large molecular gas reservoir, in a similar fashion as the 'central molecular zone' in the Milky Way, which is found to have a star formation efficiency approximately 10 times lower than the Milky Way disc. In fact, the Milky Way itself is a likely cLIER candidate, given its inferred green valley optical colours and SFR lower than the star formation main sequence (Mutch, Croton & Poole 2011).

In this context, secular evolution processes (interaction with a bar or spiral density waves) and radial flows represent a possible explanation for the presence of cold gas in the central regions of cLIERs, which is required in order to explain the observed LIER emission. The kinematic correspondence between the stars and gas, which is preserved in the central regions of cLIER galaxies, further supports a scenario where the gas in the central region of cLIER galaxies is either integral part of the disc or has been acquired from it. Indeed, the absence of line-less bulges in the current sample is a strong indication that central regions of bulge + disc systems are always more gas rich than galaxies on the red sequence and points towards the importance of the SF disc as a possible reservoir of gas in these systems.

In summary, cLIER galaxies are consistent with both a scenario of slow gas exhaustion and a scenario of reduced star formation efficiency in the bulge, driven by dynamical processes. The cold gas content of the central regions of these galaxies is not known, however some amount of gas must be present in order to allow for the observed LIER emission. This gas shares the same kinematics of the SF disc and is thus possibly driven into the central regions by bars or other disc instabilities. Followup resolved studies of the cold gas content of bulge + disc systems are needed in order to shed further light into the reasons for the absence of star formation in the central regions of cLIERs.

7.2 Ionized gas on the red sequence and the nature of eLIER galaxies

7.2.1 Origin of the gas in red galaxies

It has long been argued that red sequence galaxies have a large and plentiful source of ionized gas in their old stellar populations. Stellar evolution predicts that an old stellar population returns of the order of half its stellar mass to the ISM over a Hubble time (Ciotti et al. 1991; Padovani & Matteucci 1993; Jungwiert, Combes & Palous 2001). Mass return is dominated by stellar mass-loss during the evolution of intermediate and low-mass stars along the red giant branch and the post-AGB phases. Padovani & Matteucci (1993) predict that, for a Salpeter initial mass function, a 15 Gyr old population will lead to a mass-loss rate per unit stellar mass of

$$\dot{\mathrm{M}}_\star = 2.3 \times 10^{-12}\ \mathrm{yr}^{-1}\mathrm{M}_\star. \quad (2)$$

The mass of ionized gas can be estimated from the Hα luminosity as

$$M_{\mathrm{H\,II}} = 2.3 \times 10^3 \left(\frac{L_{\mathrm{H}\alpha}}{10^{38}\ \mathrm{erg\ s^{-1}}}\right)\left(\frac{10^2\ \mathrm{cm^{-3}}}{n_{\mathrm{e}}}\right)\mathrm{M}_\odot. \quad (3)$$

For typical integrated Hα luminosities observed in eLIERs, this implies a mass of about $\sim 10^4$–$10^5\,\mathrm{M}_\odot$. Therefore, for eLIER galaxies of typical mass of about $10^{10.5}\,\mathrm{M}_\odot$, the typical nebular line luminosities can easily be accounted for by gas injected into the ISM by stellar mass losses over a time-scale of only a few million years.

However, the kinematic signatures of the ionized gas are expected to be similar to those of the parent stars. This predictions is at odds with the observational evidence that a large fraction ($\sim$65 per cent) of eLIER galaxies are kinematically misaligned. Thus, stellar mass-loss can only be responsible for a minor fraction of the gas associated with LIER emission. Instead it is likely that the gas supplied by stellar mass-loss is quickly transferred into the hot X-ray emitting phase, with only a small fraction succeeding to cool. Indeed, the standard paradigm of the ISM in red sequence galaxies assumes that supersonic motion of the ejecta through the ambient hot medium generates a strong shock that thermalizes the gas to the kinetic temperature of the stars, $\sim 10^6$–10^7 K, on a time-scale of $\sim 10^5$–10^6 yr (Sanders 1981; Mathews 1990). Episodic AGN activity could also be responsible for balancing cooling (Ciotti & Ostriker 2007; Schawinski et al. 2007; Cheung et al. 2016) and maintaining the gas in a hot state.

In summary, the existence of a large population of red sequence galaxies with EW(Hα) < 1 Å and the same stellar population properties as eLIERs suggests that stellar mass-loss cannot be the main source of cool gas in these galaxies. This inference is confirmed by the fact that in our sample of eLIERs external accretion is required in at least 65 per cent of the population to explain the observed kinematic misalignment between gas and stars.

7.2.2 The role of environment on the red sequence

As discussed in Section 6, environmental effects are known to play a key role in determining the passive fraction of galaxies (Dressler 1980; Peng et al. 2010). In this work, we have shown that, on top of determining the passive faction, environmental effects also affect the presence of line emission and thus the cold gas content in red sequence galaxies. In particular, we have demonstrated that red sequence galaxies with small or undetected line emission [EW(Hα) < 1 Å] live in denser environments, both as centrals and satellites, than eLIERs of the same mass.

Downloaded from https://academic.oup.com/mnras/article/466/3/2570/2666397 by INAF Trieste (Osservatorio Astronomico di Trieste) user on 25 November 2020

At the high end of the stellar mass function line-less galaxies are mostly the central galaxies in high-mass haloes. Their position within a large halo would both impede accretion of external cold gas and heat up the gas recycled via stellar evolution, thus leaving the galaxy line-less. Analysis of the stellar kinematics of the MaNGA data further demonstrates that at high masses most galaxies classified as slow rotators are line-less, as expected from the kinematics–density relation (Cappellari et al. 2011b). These central, massive, slowly rotating line-less galaxies represent the striking endpoint of galaxy evolution.

At the low-mass end, environment is known to play a crucial role in making galaxies line-less, albeit via a different route (e.g. Geha et al. 2012). We demonstrate in Fig. 7 that for $M_\star < 10^{10}\,M_\odot$ more than 70 per cent of line-less galaxies are satellites, in contrast with the much lower satellite fraction for eLIERs (∼40 per cent). Satellites are generally not thought to accrete gas after falling into the hot environment of galaxy overdensities (or anyhow to accrete at a substantially lower rate than centrals, Keres et al. 2009) and are likely to undergo some amount of ram-pressure stripping as they enter a massive halo. Moreover, while at first the merger rate is enhanced as galaxies fall into rich haloes, once the galaxies virialize the large velocity dispersion within cluster considerably suppresses the subsequent merger rate (van Dokkum et al. 1999), thus making it harder to obtain gas from gas-rich mergers. While it is possible that some amount of dense gas survives the infall event and allows the satellite galaxy to continue forming stars for a time-scale comparable to the depletion time (Wetzel et al. 2013), once star formation ceases the strong environmental effects are likely to seriously disrupt the diffuse gas component and finally leave the galaxy line-less.

8 CONCLUSIONS

In this paper, we study the properties of galaxies based on their spatially resolved ionized gas emission. We make use of spatially resolved spectroscopy for a sample of 586 galaxies from SDSS-IV MaNGA, and classify galaxies according to the classification scheme introduced in Belfiore et al. (2016), which properly accounts for the ubiquitous presence of LIERs. Within this framework non-active galaxies are classified in four classes: (1) SF galaxies, (2) galaxies characterized by LIER emission at small galactocentric radii and star formation at larger radii (cLIERs), (3) galaxies characterized by LIER emission at all radii where line emission is detected (eLIERs), (4) line-less galaxies, operationally defined to have average EW(Hα) < 1 Å within $1.0\,R_e$.

In this work, we place these galaxy classes within the context of the evolving galaxy population by studying their integrated colours and SFR, morphology and kinematics. We complement the MaNGA data with environmental information for the much larger MaNGA parent sample (∼30 000 galaxies with legacy SDSS spectroscopy) to be able to disentangle the effect of mass and environment on line emission on the red sequence. In the following, we summarize the fundamental properties of the two new galaxy classes we have focused on.

Central LIER galaxies (cLIERs)

(i) Stellar populations: cLIERs span a wide range of stellar ages, with old central LIER regions and outer regions characterized by young stellar populations.

(ii) Colours and SFR: cLIERs lie preferentially in and around the green valley in UV-optical colours, although they appear increasingly consistent with the red sequence using optical colours alone ($u - r$ or $g - r$). In the SFR–$M_\star$ diagram cLIERs lie 0.8 dex below the main sequence of SF galaxies, albeit with a large scatter.

(iii) Morphology: cLIER galaxies are visually classified as disc galaxies, but have larger bulge fraction than SF galaxies of the same mass, as traced via photometric indices and spectroscopic stellar velocity dispersion measurements.

(iv) Kinematics: cLIERs display regular disc-like kinematics in both gas and stars, which are mutually aligned.

(v) Environment: cLIERs live in slightly denser environments than SF galaxies for $\log(M_\star/M_\odot) = 10.5$–$11.5$, but have the same satellite fraction.

cLIERs are consistent with originating from SF galaxies that are slowly quenching. The inside-out quenching pattern is consistent with both gas exhaustion and/or a decrease in the star formation efficiency. In either case, the presence of a bulge is closely connected to the lack of central star formation in these galaxies. The SF disc is the likely source of the LIER emitting gas present in the central regions.

Extended LIER galaxies (eLIERs)

(i) Stellar populations: eLIERs have old stellar populations, indistinguishable from those of line-less galaxies.

(ii) Colours and SFR: eLIERs lie on the red sequence in colour-magnitude diagrams, with only a small contamination to the green valley.

(iii) Morphology: eLIER galaxies are visually classified as ETGs and have similar bulges to those of line-less galaxies of the same stellar mass.

(iv) Kinematics: eLIERs display a variety of gas kinematics, but generally present well-defined rotation/flows on kpc scales. The velocity field of gas and stars are often observed to be misaligned (65 ± 7 per cent of eLIERs are misaligned by more than 30°).

(v) Environment: eLIERs live in denser environments than SF and cLIERs at high masses ($M_\star > 10^{10.5}\,M_\odot$), as expected from the well-known correlation between colour and passive fraction. More importantly eLIERs tend to live in less dense environments than line-less galaxies of the same mass. At the high-mass end, line-less galaxies are mostly centrals in high-mass haloes, while at the low-mass end line-less galaxies are mostly satellites.

eLIERs are red sequence galaxies with residual cold gas, acquired mostly via external sources. While this gas does not form stars, it is illuminated by the diffuse ionization field from hot old stars and shines with LIER line ratios. LIER emission is suppressed in high-density environments, likely because of lack of gas, which has either been consumed due to the shutdown of inflows or otherwise heated and/or tidally stripped by the hot halo gas.

ACKNOWLEDGEMENTS

We are grateful to the referee, A. Renzini, for his comments and insight that have greatly improved the quality of the paper. FB, RM and KM acknowledge funding from the United Kingdom Science and Technology Facilities Council (STFC). RM acknowledges support from the European Research Council (ERC) Advanced Grant 695671 'QUENCH'. AR-L acknowledges partial support from the DIULS regular project PR15143. MB was supported by NSF/AST-1517006. KB was supported by World Premier International Research Centre Initiative (WPI Initiative), MEXT,

Downloaded from https://academic.oup.com/mnras/article/466/3/2570/2666397 by INAF Trieste (Osservatorio Astronomico di Trieste) user on 25 November 2020

Japan and by JSPS KAKENHI Grant Number 15K17603. AW acknowledges support from a Leverhulme Early Career Fellowship. AD acknowledges support from The Grainger Foundation. The authors are thankful to Y. Peng and D. Goddard for their help with the environmental measures for the SDSS galaxy sample and to M. Blanton for developing and maintaining the NASA-Sloan Atlas; to the members of the SDSS-IV MaNGA collaboration, in particular the dedicated team of observers at APO. The visual classification of the Galaxy Zoo galaxies was made by more than 100 000 volunteers. Their contributions are acknowledged at http://www.galaxyzoo.org/Volunteers.aspx. This work makes use of data from SDSS-I–II and IV. This research made use of Marvin (Cherinka et al. in preparation), a core Python package and web framework for MaNGA data, developed by Brian Cherinka, José Sánchez-Gallego and Brett Andrews.

Funding for SDSS-I-II and SDSS-IV has been provided by the Alfred P. Sloan Foundation and Participating Institutions. Additional funding for SDSS-II comes the National Science Foundation, the U.S. Department of Energy, the National Aeronautics and Space Administration, the Japanese Monbukagakusho, the Max Planck Society and the Higher Education Funding Council for England. Additional funding towards SDSS-IV has been provided by the U.S. Department of Energy Office of Science. SDSS-IV acknowledges support and resources from the Centre for High-Performance Computing at the University of Utah. The SDSS web site is www.sdss.org.

The participating Institution in SDSS-II include the American Museum of Natural History, Astrophysical Institute Potsdam, University of Basel, University of Cambridge, Case Western Reserve University, University of Chicago, Drexel University, Fermilab, the Institute for Advanced Study, the Japan Participation Group, Johns Hopkins University, the Joint Institute for Nuclear Astrophysics, the Kavli Institute for Particle Astrophysics and Cosmology, the Korean Scientist Group, the Chinese Academy of Sciences (LAMOST), Los Alamos National Laboratory, Max-Planck-Institut für Astronomie (MPIA Heidelberg), Max-Planck-Institut für Astrophysik (MPA Garching), New Mexico State University, Ohio State University, University of Pittsburgh, University of Portsmouth, Princeton University, the United States Naval Observatory and the University of Washington.

SDSS-IV is managed by the Astrophysical Research Consortium for the Participating Institutions of the SDSS Collaboration including the Brazilian Participation Group, the Carnegie Institution for Science, Carnegie Mellon University, the Chilean Participation Group, the French Participation Group, Harvard-Smithsonian Center for Astrophysics, Instituto de Astrofísica de Canarias, The Johns Hopkins University, Kavli Institute for the Physics and Mathematics of the Universe (IPMU)/University of Tokyo, Lawrence Berkeley National Laboratory, Leibniz Institut für Astrophysik Potsdam (AIP), Max-Planck-Institut für Astronomie (MPIA Heidelberg), Max-Planck-Institut für Astrophysik (MPA Garching), Max-Planck-Institut für Extraterrestrische Physik (MPE), National Astronomical Observatory of China, New Mexico State University, New York University, University of Notre Dame, Observatário Nacional/MCTI, The Ohio State University, Pennsylvania State University, Shanghai Astronomical Observatory, United Kingdom Participation Group, Universidad Nacional Autónoma de México, University of Arizona, University of Colorado Boulder, University of Oxford, University of Portsmouth, University of Utah, University of Virginia, University of Washington, University of Wisconsin, Vanderbilt University and Yale University.

All data taken as part of SDSS-IV is scheduled to be released to the community in fully reduced form at regular intervals through dedicated data releases. The MaNGA data used in this work is part of SDSS data release 13 (Albareti et al. 2016), publicly available at http://www.sdss.org/dr13/manga/manga-data/.

REFERENCES

Abazajian K. N. et al., 2009, ApJS, 182, 543
Albareti F. D. et al., 2016, preprint (arXiv:e-prints)
Allen J. T. et al., 2015, MNRAS, 446, 1567
Baldry I. K., Glazebrook K., Brinkmann J., Ivezic Z., Lupton R. H., Nichol R. C., Szalay A. S., 2004, ApJ, 600, 681
Baldry I. K., Balogh M. L., Bower R. G., Glazebrook K., Nichol R. C., Bamford S. P., Budavari T., 2006, MNRAS, 373, 469
Baldwin J. A., Phillips M. M., Terlevich R., 1981, PASP, 93, 5
Balogh M. L., Morris S. L., Yee H. K. C., Carlberg R. G., Ellingson E., 1999, ApJ, 527, 54
Balogh M. L., Baldry I. K., Nichol R. C., Miller C., R B., Glazebrook K., 2004, ApJ, 615, L101
Bamford S. P. et al., 2009, MNRAS, 393, 1324
Belfiore F. et al., 2015, MNRAS, 449, 867
Belfiore F. et al., 2016, MNRAS, 461, 3111 (Paper I)
Bell E. F. et al., 2012, ApJ, 753, 167
Bertola F., Corsini E. M., Vega Beltran J. C., Pizzella A., Sarzi M., Cappellari M. J. G., Funes S., 1999, ApJ, 519, L127
Binette L., Magris C. G., Stasińska G., Bruzual A. G., 1994, A&A, 292, 13
Birnboim Y., Dekel A., 2003, MNRAS, 345, 349
Blanc G. A., Heiderman A., Gebhardt K., Evans N. J., Adams J., 2009, ApJ, 704, 842
Blanton M. R., Moustakas J., 2009, Annu. Rev. Astron. Astrophys., 47, 159
Blanton M. R., Roweis S., 2007, AJ, 133, 734
Blanton M. R. et al., 2003, ApJ, 594, 186
Blanton M. R. et al., 2005a, AJ, 129, 2562
Blanton M., Eisenstein D., Hogg D., Schlegel D., Brinkmann J., 2005b, ApJ, 629, 143
Blanton M. R., Kazin E., Muna D., Weaver B. A., Price-Whelan A., 2011, AJ, 142, 31
Bluck A. F. L., Mendel J. T., Ellison S. L., Moreno J., Simard L., Patton D. R., Starkenburg E., 2014, MNRAS, 441, 599
Boselli A., Cortese L., Boquien M., 2014, A&A, 564, A65
Bower R. G., Benson A. J., Malbon R., Helly J. C., Frenk C. S., Baugh C. M., Cole S., Lacey C. G., 2006, MNRAS, 370, 645
Brinchmann J., Charlot S., White S. D. M., Tremonti C., Kauffmann G., Heckman T., Brinkmann J., 2004, MNRAS, 351, 1151
Brown T., Ferguson H., Stanford S., Deharveng J.-M., 1998, ApJ, 504, 113
Brown T. M., Smith E., Ferguson H. C., Sweigart A. V., Kimble R. A., Bowers C. W., 2008, ApJ, 682, 319
Bruzual G., Charlot S., 2003, MNRAS, 344, 1000
Bundy K. et al., 2010, ApJS, 719, 1969
Bundy K. et al., 2015, ApJ, 798, 7
Calzetti D., 2001, PASP, 113, 1449
Cappellari M., 2016, Annu. Rev. Astron. Astrophys., 54, 1
Cappellari M., Emsellem E., 2004, PASP, 116, 138
Cappellari M. et al., 2011a, MNRAS, 413, 813
Cappellari M. et al., 2011b, MNRAS, 416, 1680
Cappellari M. et al., 2013, MNRAS, 432, 1862
Cardelli J. A., Clayton G. C., Mathis J. S., 1989, ApJ, 345, 245
Carniani S. et al., 2015, A&A, 580, A102
Carollo et al., 2016, ApJ, 818, 180
Cattaneo A. et al., 2009, Nature, 460, 213
Chabrier G., 2003, PASP, 115, 763
Cheung E. et al., 2012, ApJ, 760, 131
Cheung E. et al., 2013, ApJ, 779, 162
Cheung E. et al., 2016, Nature, 533, 504
Chung A., van Gorkom J. H., Kenney J. D. P., Crowl H., Vollmer B., 2009, AJ, 138, 1741

Downloaded from https://academic.oup.com/mnras/article/466/3/2570/2666397 by INAF Trieste (Osservatorio Astronomico di Trieste) user on 25 November 2020

Cicone C. et al., 2014, A&A, 562, A21
Ciotti L., Ostriker J. P., 2007, ApJ, 665, 1038
Ciotti L., D'Ercole A., Pellegrini S., Renzini A., 1991, ApJ, 376, 380
Cortese L., Catinella B., Boissier S., Boselli A., Heinis S., 2011, MNRAS, 415, 1797
Croton D. J. et al., 2006, MNRAS, 365, 11
Davis T. A., Bureau M., 2016, MNRAS, 457, 272
Davis T. A. et al., 2011, MNRAS, 417, 882
Davis T. A. et al., 2014, MNRAS, 444, 3427
De Lucia G., Fontanot F., Wilman D., Monaco P., 2011, MNRAS, 414, 1439
Dekel A., Birnboim Y., 2006, MNRAS, 368, 2
Dressler A., 1980, ApJ, 236, 351
Driver S. P. et al., 2011, MNRAS, 413, 971
Drory N. et al., 2015, AJ, 149, 77
Elmegreen B. G., 1995, MNRAS, 275, 944
Emsellem E. et al., 2007, MNRAS, 379, 401
Emsellem E. et al., 2011, MNRAS, 414, 888
Emsellem E., Renaud F., Bournaud F., Elmegreen B., Combes F., Gabor J., 2015, MNRAS, 446, 2468
Etherington J., Thomas D., 2015, MNRAS, 451, 660
Fabian A., 2012, ARA&A, 50, 455
Fanali R., Dotti M., Fiacconi D., Haardt F., 2015, MNRAS, 454, 3641
Forbes J. C., Krumholz M. R., Burkert A., Dekel A., 2014, MNRAS, 438, 1552
Franx M., Illingworth G., de Zeeuw T., 1991, ApJ, 383, 112
Fumagalli M., Fossati M., Hau G. K. T., Gavazzi G., Bower R., Sun M., Boselli A., 2014, MNRAS, 445, 4335
Gabor J. M., Davé R., 2012, MNRAS, 427, 1816
Geha M., Blanton M. R., Yan R., Tinker J. L., Haven N., 2012, ApJ, 85, 85
Genzel R. et al., 2014, ApJ, 785, 75
Gerhard O., Binney J., 1996, MNRAS, 279, 993
Gomes J. M., Papaderos P., Vílchez J. M., Kehrig C., Breda I., Lehnert M. D., 2016, A&A, 585, A92
Gunn J. E., Gott J. R., 1972, ApJ, 176, 1
Gunn J. E. et al., 2006, AJ, 131, 2332
Häring N., Rix H.-W., 2004, ApJ, 604, L89
Heckman T. M., Best P. N., 2014, ARA&A, 52, 589
Jog C. J., Solomon P. M., 1984, ApJ, 276, 127
Jungwiert B., Combes F., Palous J., 2001, A&A, 35, 85
Kauffmann G. et al., 2003a, MNRAS, 341, 33
Kauffmann G. et al., 2003b, MNRAS, 341, 54
Kauffmann G. et al., 2003c, MNRAS, 346, 1055
Kauffmann G., Heckman T. M., De Lucia G., Brinchmann J., Charlot S., Tremonti C., White S. D. M., Brinkmann J., 2006, MNRAS, 367, 1394
Kennicutt R. C., 1998, ARA&A, 36, 189
Keres D., Katz N., Weinberg D. H., Davé R., 2005, MNRAS, 363, 2
Kereš D., Katz N., Fardal M., Davé R., Weinberg D. H., 2009, MNRAS, 395, 160
Kewley L. J., Ellison S. L., 2008, ApJ, 681, 1183
Knobel C., Lilly S. J., Woo J., Kovač K., 2015, ApJ, 800, 24
Kormendy J., Drory N., Bender R., Cornell M. E., 2010, ApJ, 723, 54
Krajnovic D., Cappellari M., De Zeeuw P. T., Copin Y., 2006, MNRAS, 366, 787
Krajnović D. et al., 2013, MNRAS, 432, 1768
Lake G., Norman C., 1983, ApJ, 270, 51
Larson R. B., Tinsley B. M., Caldwell C. N., 1980, ApJ, 237, 692
Law D. R. et al., 2015, AJ, 150, 19
Law D. R. et al., 2016, AJ, 152, 83
Leroy A. K., Walter F., Brinks E., Bigiel F., de Blok W. J. G., Madore B., Thornley M. D., 2008, AJ, 136, 2782
Li C. et al., 2015, ApJ, 804, 125
Lilly S. J. et al., 2007, ApJS, 172, 70
Lintott C. J. et al., 2008, MNRAS, 389, 1179
Longmore S. N. et al., 2013, MNRAS, 429, 987
Maiolino R. et al., 2012, MNRAS, 425, L66
Maraston C., Stromback G., 2011, MNRAS, 418, 2785
Marconi A., Hunt L. K., 2003, ApJ, 589, L21
Martig M., Bournaud F., Teyssier R., Dekel A., 2009, ApJ, 707, 250
Martig M. et al., 2013, MNRAS, 432, 1914
Masters K. L. et al., 2010, MNRAS, 405, 783
Masters K. L. et al., 2011, MNRAS, 418, 1055
Masters K. L. et al., 2012, MNRAS, 424, 2180
Mathews W. G., 1990, ApJ, 354, 468
McConnell N. J., Ma C.-P., 2013, ApJ, 764, 184
Mendel T. J., Simard L., Ellison S. L., Patton D. R., 2013, MNRAS, 429, 2212
Mutch S. J., Croton D. J., Poole G. B., 2011, ApJ, 736, 84
Nair P. B., Abraham R. G., 2010, ApJ, 714, L260
O'Donnell J. E., 1994, ApJ, 422, 158
Osterbrock D. E., Ferland G. J., 2006, Astrophysics of Gaseous Nebulae and Active Galactic Nuclei. University Science Books, Mill Valley, CA
Padovani P., Matteucci F., 1993, ApJ, 416, 26
Pasquali A., Gallazzi A., van den Bosch F. C., 2012, MNRAS, 425, 273
Peng Y.-j. et al., 2010, ApJ, 721, 193
Peng Y., Maiolino R., Cochrane R., 2015, Nature, 521, 192
Poggianti B. M. et al., 2016, AJ, 151, 78
Rees M., Ostriker J., 1977, MNRAS, 179, 541
Renzini A., Peng Y.-j., 2015, ApJ, 801, L29
Romeo A. B., Wiegert J., 2011, MNRAS, 416, 1191
Rosenfield P. et al., 2012, ApJ, 755, 131
Rybicki G., 1987, in de Zeeuw P., ed., IAU Symp. Vol. 127, Structure and Dynamics of Elliptical Galaxies. D. Reidel Publishing Co., Dordrecht, p. 397
Saintonge A. et al., 2011, MNRAS, 415, 61
Saintonge A. et al., 2012, ApJ, 758, 73
Sales L. V. et al., 2014, MNRAS, 447, L6
Salim S. et al., 2007, ApJS, 173, 267
Sánchez S. F. et al., 2012, A&A, 538, A8
Sandage A., 1961, The Hubble Atlas of Galaxies. Carnegie Institution, Washington
Sanders R., 1981, ApJ, 244, 820
Sarzi M. et al., 2006, MNRAS, 366, 1151
Sarzi M. et al., 2010, MNRAS, 402, 2187
Schawinski K., Thomas D., Sarzi M., Maraston C., Kaviraj S., Joo S. J., Yi S. K., Silk J., 2007, MNRAS, 382, 1415
Schawinski K. et al., 2014, MNRAS, 440, 889
Schaye J. et al., 2014, MNRAS, 446, 521
Silk J., 1977, ApJ, 211, 638
Simmons B. D. et al., 2013, MNRAS, 429, 2199
Singh R. et al., 2013, A&A, 558, A43
Smee S. A. et al., 2013, AJ, 146, 32
Smethurst R. J. et al., 2015, MNRAS, 450, 435
Stasińska G., Asari N. V., Cid Fernandes R., Gomes J. M., Schlickmann M., Mateus A., Schoenell W., Sodré L., Jr, 2008, MNRAS, 33, 29
Strateva I., Ivezic Z., Knapp G. R., Narayanan V. K., Strauss M. A., 2001, AJ, 122, 1861
Strauss M. A., Weinberg D. H., Lupton R. H., Narayanan V. K., 2002, AJ, 124, 1810
Tacchella A. S., Carollo C. M., Renzini A., Schreiber N. M. F., Lang P., 2015, Science, 348, 314
Thomas D., Maraston C., Korn A., 2004, MNRAS, 351, L19
Thomas D., Maraston C., Schawinski K., Sarzi M., Silk J., 2010, MNRAS, 404, 1775
Thomas D., Maraston C., Johansson J., 2011, MNRAS, 412, 2183
Tohline J. E., Durisen R. H., 1982, ApJ, 257, 94
Tojeiro R. et al., 2013, MNRAS, 432, 359
Toomre A., 1964, ApJ, 139, 1217
Trayford J. W., Theuns T., Bower R. G., Crain R. A., Lagos C. d. P., Schaller M., Schaye J., 2016, MNRAS, 460, 3925
Tremonti C. A., Heckman T. M., Kauffmann G., Brinchmann J., White S. D. M., Seibert M., Peng E. W., Schlegel D. J., 2004, ApJ, 613, 898
van de Voort F., Davis T. A., Kereš D., Quataert E., Faucher-Gigueré C. A., Hopkins P. F., 2015, MNRAS, 451, 3269
van den Bergh S., 1976, ApJ, 206, 883

Downloaded from https://academic.oup.com/mnras/article/466/3/2570/2666397 by INAF Trieste (Osservatorio Astronomico di Trieste) user on 25 November 2020

van Dokkum P. G., Franx M., Fabricant D., Kelson D. D., Illingworth G. D., 1999, ApJ, 520, L95
Vazdekis A., Ricciardelli E., Cenarro A. J., Rivero-González J. G., Díaz-García L. A., Falcón-Barroso J., 2012, MNRAS, 424, 157
Vogelsberger M. et al., 2014, MNRAS, 444, 1518
Wake D. A., van Dokkum P. G., Franx M., 2012, ApJ, 751, L44
Wetzel A. R., Tinker J. L., Conroy C., van den Bosch F. C., 2013, MNRAS, 432, 336
Wilkinson D. M. et al., 2015, MNRAS, 449, 328
Willett K. W. et al., 2013, MNRAS, 435, 2835
Wisnioski E. et al., 2015, ApJ, 799, 209
Wolf C. et al., 2009, MNRAS, 393, 1302
Wyder T. K. et al., 2007, ApJS, 173, 293
Yan R., Blanton M. R., 2012, ApJ, 747, 61
Yan R. et al., 2016a, AJ, 152, 197
Yan R. et al., 2016b, AJ, 151, 8
Yang X., Mo H. J., van der Bosch F. C., Jing Y. P., 2005, MNRAS, 356, 1293
Yang X., Mo H. J., van den Bosch F. C., Pasquali A., Li C., Barden M., 2007, ApJ, 671, 153
York D. G. et al., 2000, AJ, 120, 1579

SUPPORTING INFORMATION

Supplementary data are available at *MNRAS* online.

Table B1. Identifiers and fundamental properties of the galaxy sample used in this work.
Table B2. Photometric and morphological properties for the galaxy sample used in this work.

Please note: Oxford University Press is not responsible for the content or functionality of any supporting materials supplied by the authors. Any queries (other than missing material) should be directed to the corresponding author for the article.

APPENDIX A: COMPUTING THE STAR FORMATION RATE

In this work, we compute the SFR using the extinction-corrected Hα flux from the MaNGA data. We calculate the reddening from the Balmer decrement, by using the Hα/Hβ ratio and a Calzetti (2001) attenuation curve with $R_V = 4.05$. The theoretical value for the Balmer line ratio is taken from Osterbrock & Ferland (2006), assuming case B recombination (Hα/Hβ = 2.87). We note that the use of extinction curve of Cardelli, Clayton & Mathis (1989) (or the modification by O'Donnell 1994) with $R_V = 3.1$ yields very similar results for the 3600 to 7000 Å wavelength range considered in this work.

The simplest approach to computing SFR would be to exclude regions (spaxels) that are not classified as SF by making use of a hard cut on a BPT diagnostic diagram. We consider this approach partly unsatisfactory because of the rather arbitrary nature of the demarcation lines. Instead we suggest a framework where the total Hα flux is the combination of a contribution from H II regions, related to star formation, and a contribution from old evolved stars (LIERs) and LIER-like diffuse ionized gas. In order to disentangle the two components we rely on their different lines ratios, following a similar approach to Blanc et al. (2009). In this work we choose to use [S II]/Hα, which is the most sensitive line ratio to the presence of LIER emission studied in Paper I. Defining f_{SF} to be the fraction of Hα flux due to star formation and f_L the fraction of Hα flux due to LIERs, we have

$$f_{SF} + f_L = 1,$$
$$\left(\frac{[S\,II]}{H\alpha}\right) = f_{SF}\left(\frac{[S\,II]}{H\alpha}\right)_{SF} + f_L\left(\frac{[S\,II]}{H\alpha}\right)_L \quad (A1)$$

where $\left(\frac{[S\,II]}{H\alpha}\right)_{SF} = 0.4$ and $\left(\frac{[S\,II]}{H\alpha}\right)_L = 0.9$ are the characteristic line ratios for SF regions and LIERs, respectively, whose numerical values are obtained in Paper I, as the representative line ratio values for SF and eLIER galaxies respectively. To calculate the SFR, we solve for f_{SF} for each spaxel and then sum the total Hα luminosity due to star formation within the FoV of each MaNGA galaxy. We convert the Hα luminosity to SFR using the conversion factor from Kennicutt (1998). We note that this approach leads to very similar numerical results to a hard cut on SF spaxels based on a BPT demarcation line. For example, using the same demarcation line as Paper I on the [S II] BPT diagram to classify SF spaxels and only using those spaxels in the SFR calculation leads to SFR that strongly correlate with our estimate for purely SF galaxies (Pearson correlation coefficient of 0.997). The SFR calculated using the LIER correction is, on average, systematically larger by only 0.03 dex from that computed using only SF spaxels with a average scatter of 0.07 dex.

Our SFR estimates are also in excellent agreement with the SFR reported in the MPA-JHU catalogue (Brinchmann et al. 2004), based on legacy SDSS spectroscopy (Pearson correlation coefficient of 0.8, dispersion of 0.4 dex). As shown in Fig. A1 , the offset from the one-to-one relation is substantially larger for cLIERs (0.5 dex) than SF galaxies (0.07 dex), which is not surprising given the poor leverage of the SDSS 3 arcsec fibre in calculating the SFR in cLIERs. Further details on the SFR estimators for MaNGA galaxies and aperture corrections is beyond the scope of this section and will be presented in future work.

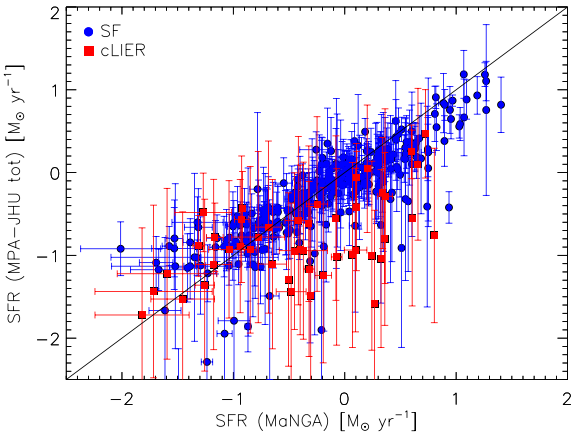


Figure A1. The relation between the SFR estimates from the MPA-JHU catalogue (Brinchmann et al. 2004) based on legacy SDSS spectroscopy and MaNGA (as calculated in this work) for SF and cLIER galaxies. The one-to-one relation is highlighted with a black solid line.

APPENDIX B: ADDITIONAL MATERIAL

We present here SDSS $g - r - i$ composite images and Hα flux maps all the cLIER and eLIER galaxies used in this work.

Downloaded from https://academic.oup.com/mnras/article/466/3/2570/2666397 by INAF Trieste (Osservatorio Astronomico di Trieste) user on 25 November 2020

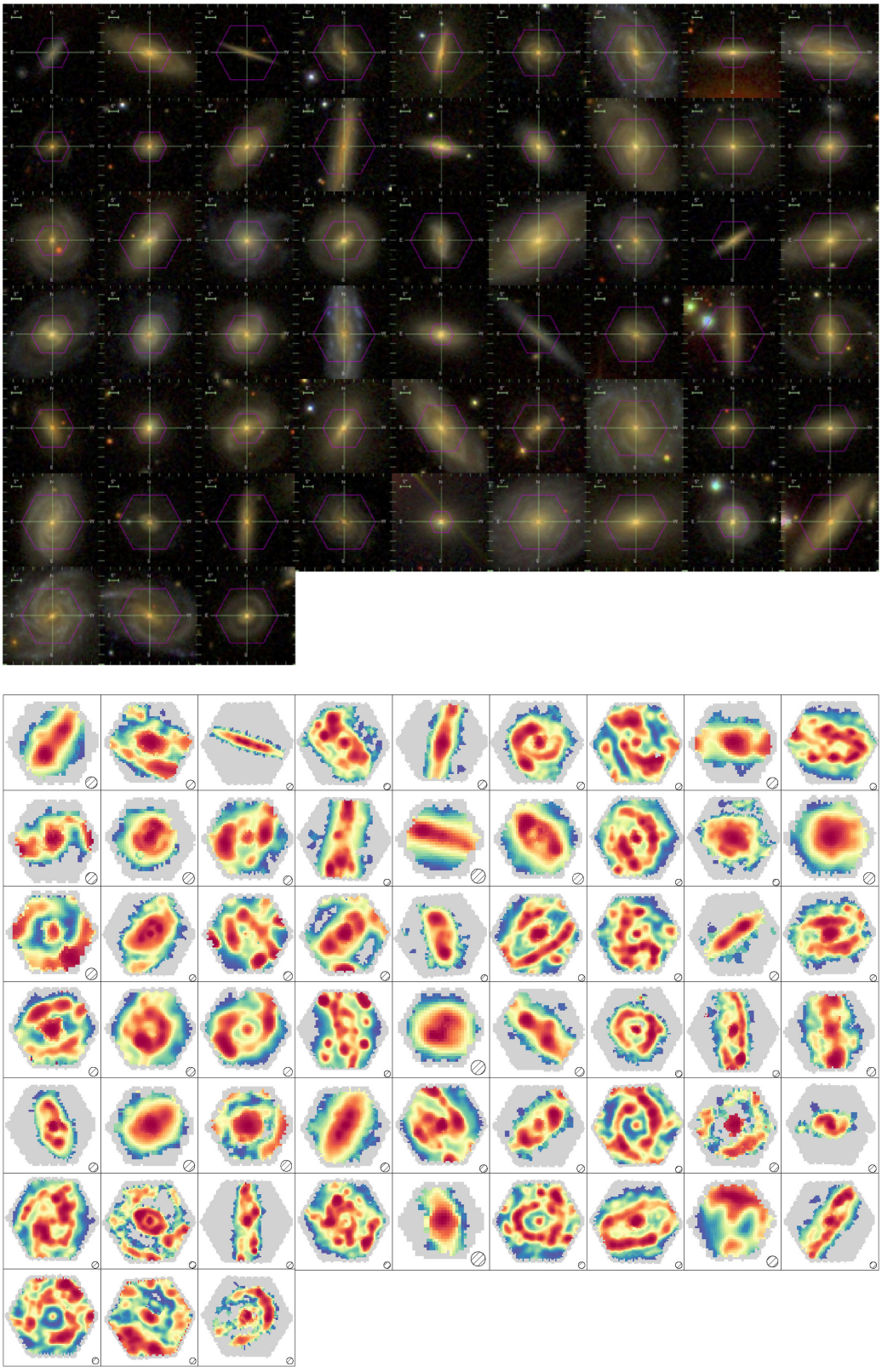


Figure B1. *Top*: SDSS $g - r - i$ colour composite images (with MaNGA IFU bundle FoV superimposed) for the sample of cLIER galaxies studied in this work. *Bottom*: MaNGA Hα flux maps for the sample of cLIER galaxies studied in this work.

Downloaded from https://academic.oup.com/mnras/article/466/3/2570/2666397 by INAF Trieste (Osservatorio Astronomico di Trieste) user on 25 November 2020

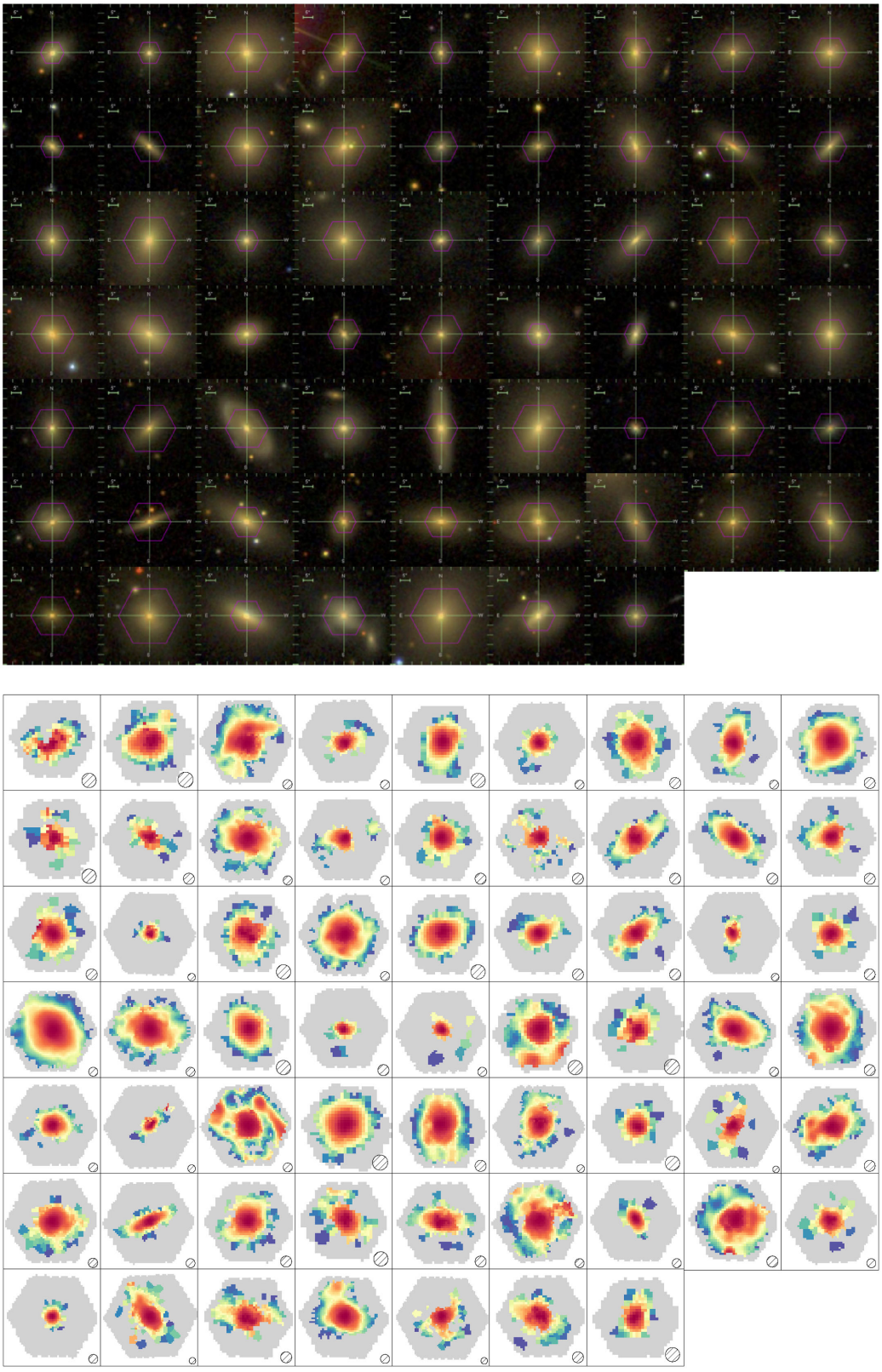


Figure B2. *Top*: SDSS $g - r - i$ colour composite images (with MaNGA IFU bundle FoV superimposed) for the sample of eLIER galaxies studied in this work. *Bottom*: MaNGA Hα flux maps for the sample of eLIER galaxies studied in this work.

Downloaded from https://academic.oup.com/mnras/article/466/3/2570/2666397 by INAF Trieste (Osservatorio Astronomico di Trieste) user on 25 November 2020

Table B1. Identifiers and fundamental properties of the galaxy sample used in this work. Table for the full sample available online.

MaNGA-ID	NSA-ID	RA J2000 deg	Dec J2000 deg	z	Plate	IFU design	$\log(M_\star)$ ($M_\odot$)	log(SFR) ($M_\odot$ yr^{-1})	R_e (arcsec)	EM class
1-23929	25589	259.174713	56.927792	0.028	7991	9101	10.086	-0.353	8.768	SF
1-24006	25673	257.833832	56.991253	0.031	7991	6103	9.734	-0.356	5.565	SF
1-24099	25775	258.027618	57.504009	0.028	7991	1902	10.462	NaN	3.624	eLIER
1-24124	25801	258.530273	57.477432	0.027	7991	3703	9.768	NaN	4.818	LL
1-24354	26050	261.083344	56.876629	0.028	7991	6102	9.900	NaN	6.634	LL
1-24368	26065	261.321045	56.951878	0.025	7991	12704	10.042	−0.317	12.865	SF
1-25819	27618	259.874573	55.432957	0.072	7991	3701	11.069	<−1.256	3.073	LL
1-25911	27716	260.346985	55.876526	0.140	7991	9102	11.471	NaN	6.755	LL
1-37965	40459	48.642723	0.532375	0.021	8082	9101	9.432	−1.614	8.656	SF
1-37973	40468	49.108551	0.321643	0.021	8082	3702	9.258	−1.311	5.266	cLIER
...										

Column notes:(1) MaNGA-ID is the primary identifier denoting a unique galaxy within the MaNGA survey; (2) NSA-ID is the identification number of the MaNGA galaxy target from the NSA parent catalogue; (3–5) taken from NSA; (6–7) the combination of plate and IFU design uniquely identifies each MaNGA observation (equivalent to the plate-fibre-MJD spectral identifiers from legacy SDSS); (8) $M_\star$ from fit to the integrated photometry from the NSA; (9) SFR from MaNGA data, as computed in this work; (10) half-light radius from a Sérsic fit to the *r*-band legacy SDSS photometry, from the NSA; (11) emission-line class as defined in this work: SF – star forming, cLIER – central LIER, eLIER – extended LIER, LL – line-less.

Table B2. Photometric and morphological properties for the galaxy sample used in this work. Table for the full sample available online.

MaNGA-ID	*b/a* Sérsic	*n* Sérsic	ϕ Sérsic (deg)	R_{90}/R_{50}	GZ p_{disc}	$\sigma_\star(0.5\,R_e)$ (km s^{-1})	$NUV-r$ (mag)	$u-r$ (mag)	$g-r$ (mag)
1-23929	0.366	1.008	12.278	2.389	0.420	55.170	3.260	1.986	0.651
1-24006	0.259	0.829	177.225	2.532	0.774	53.330	3.108	1.754	0.579
1-24099	0.666	3.893	127.189	3.029	0.077	123.840	5.497	2.344	0.738
1-24124	0.446	1.100	37.710	2.351	0.113	56.480	4.748	2.085	0.625
1-24354	0.288	0.616	61.907	2.007	0.978	65.840	5.422	2.391	0.731
1-24368	0.725	1.904	173.668	2.949	0.530	44.620	2.419	1.612	0.543
1-25819	0.586	6.000	101.348	3.279	0.237	361.190	5.707	2.832	0.853
1-25911	0.787	5.115	88.744	3.384	0.549	226.980	6.369	2.367	0.577
1-37965	0.901	1.153	137.144	3.110	0.981	29.830	2.671	1.406	0.449
1-37973	0.251	1.412	146.287	2.545	0.896	43.310	2.397	1.693	0.617
...									

Column notes:(1) MaNGA-ID, same as above; (2) major to minor axis ratio of the Sérsic fit to the legacy SDSS *r* band, from the NSA; (3) Sérsic index of the fit, from the NSA; (4) position angle of the Sérsic fit, from the NSA; (5) concentration parameter (R_{90} and R_{50} are Petrosian radii containing respectively 90 and 50 per cent of the *r*-band light), from the NSA; (6) de-biased probability of the galaxy containing a disc, from Galaxy Zoo 2 Willett et al. (2013); (7) average stellar velocity dispersion within 0.5 R_e, from MaNGA data; (8–10) $NUV-r$, $u-r$ and $g-r$ colours from the NSA.

[1]*University of Cambridge, Cavendish Astrophysics, Cambridge CB3 0HE, UK*
[2]*University of Cambridge, Kavli Institute for Cosmology, Cambridge CB3 0HE, UK*
[3]*Institute of Cosmology and Gravitation, University of Portsmouth, Dennis Sciama Building, Portsmouth PO1 3FX, UK*
[4]*European Southern Observatory, Karl-Schwarzchild-str, 2, Garching b. Munchen D-85748, Germany*
[5]*Université Lyon 1, Observatoire de Lyon, Centre de Recherche Astrophysique de Lyon and Ecole Normale Supérieure de Lyon, 9 avenue Charles André, Saint-Genis Laval F-69230, France*
[6]*Department of Astronomy, University of Winsconsin-Madison, 475 N. Charter Street, Madison, WI 53706-1582, USA*
[7]*South East Physics Network (SEPNet), www.sepnet.ac.uk*
[8]*Sternberg Astronomical Institute, Moscow State University, 119992 Moscow, Russia*
[9]*Apache Point Observatory and New Mexico State University, PO Box 59, Sunspot, NM 88349-0059, USA*
[10]*Universidad de Antofagasta, Unidad de Astronomía, Avenida Angamos 601, Antofagasta 1270300, Chile*
[11]*Department of Physics and Astronomy, University of Utah, 115 S. 1400 E., Salt Lake City, UT 84112, USA*
[12]*Kavli Institute for the Physics and Mathematics of the Universe (WPI), The University of Tokyo Institutes for Advanced Study, The University of Tokyo, Kashiwa, Chiba 277-8583, Japan*
[13]*Department of Physics and Astronomy, Bates College, Lewiston, ME 04240, USA*
[14]*McDonald Observatory, The University of Texas at Austin, 2515 Speedway, Stop C1402, Austin, TX 78712, USA*
[15]*Center for Astrophysical Sciences, Department of Physics and Astronomy, The Johns Hopkins University, Baltimore, MD 21218, USA*
[16]*Space Telescope Science Institute, 3700 San Martin Drive, Baltimore, MD 21218, USA*
[17]*Departamento de Fisica, Facultad de Ciencias, Universidad de La Serena, Cisternas 1200, La Serena, Chile*
[18]*School of Physics and Astronomy, University of St. Andrews, North Haugh, St. Andrews KY16 9SS, UK*
[19]*Department of Physics and Astronomy, University of Kentucky, 505 Rose Street, Lexington, KY 40506-0055, USA*

This paper has been typeset from a TEX/LATEX file prepared by the author.

Downloaded from https://academic.oup.com/mnras/article/466/3/2570/2666397 by INAF Trieste (Osservatorio Astronomico di Trieste) user on 25 November 2020